Geoscience Frontiers 9 (2018) 769–788

HOSTED BY

Contents lists available at ScienceDirect

China University of Geosciences (Beijing)

Geoscience Frontiers

journal homepage: www.elsevier.com/locate/gsf

Research Paper

Geochemical systematics of the Mauranipur-Babina greenstone belt, Bundelkhand Craton, Central India: Insights on Neoarchean mantle plume-arc accretion and crustal evolution

S.P. Singh [a], K.S.V. Subramanyam [b], C. Manikyamba [b,*], M. Santosh [c,d], M. Rajanikanta Singh [b], B. Chandan Kumar [e]

[a] Department of Geology, Institute of Earth Sciences, Bundelkhand University, Jhansi, U.P, 284128, India
[b] CSIR-National Geophysical Research Institute, Uppal Road, Hyderabad, 500007, India
[c] Department of Earth Sciences, University of Adelaide, Australia
[d] School of Earth Science & Resources, China University of Geosciences, Beijing, China
[e] Department of Geology, Central University of Kerala, Kasaragod, Kerala, 671316, India

ARTICLE INFO

Article history:
Received 1 February 2017
Received in revised form
8 August 2017
Accepted 29 August 2017
Available online 16 October 2017

Keywords:
Bundelkhand craton
Greenstone belts
Mantle dynamics
Plume-arc accretion
Neoarchean crustal evolution

ABSTRACT

The Neoarchean Bundelkhand greenstone sequences at Mauranipur and Babina areas within the Bundelkhand Gneissic Complex preserve a variety of magmatic rocks such as komatiitic basalts, basalts, felsic volcanic rocks and high-Mg andesites belonging to the Baragaon, Raspahari and Koti Formations. The intrusive and extrusive komatiitic basalts are characterized by low SiO_2 (39–53 wt.%), high MgO (18–25 wt.%), moderately high Fe_2O_3 (7.1–11.6 wt.%), Al_2O_3 (4.5–12.0 wt.%), and TiO_2 (0.4–1.23 wt.%) with super to subchondritic $(Gd/Yb)_N$ ratios indicating garnet control on the melts. The intrusive komatiitic suite of Ti-enriched and Al-depleted type possesses predominant negative Eu and positive Nb, Ti and Y anomalies. The chemical composition of basalts classifies them into three types with varying SiO_2, TiO_2, MgO, Fe_2O_3, Al_2O_3 and CaO. At similar SiO_2 content of type I and III basalts, the type II basalts show slightly high Al_2O_3 and Fe_2O_3 contents. Significant negative anomalies of Nb, Zr, Hf and Ti, slightly enriched LREE with relatively flat HREE and low $\sum$REE contents are observed in type I and II basalts. Type III basalts show high Zr/Nb ratios (9.8–10.4), TiO_2 (1.97–2.04 wt.%), but possess strikingly flat Zr, Hf, Y and Yb and are uncontaminated. Andesites from Agar and Koti have high SiO_2 (55–64 wt.%), moderate TiO_2 (0.4–0.7 wt.%), slightly low Al_2O_3 (7–11.9 wt.%), medium to high MgO (3–8 wt.%) and CaO contents (10–17 wt.%). Anomalously high Cr, Co and Ni contents are observed in the Koti rhyolites. Tholeiitic to calc alkaline affinity of mafic-felsic volcanic rocks and basalt–andesite–dacite–rhyolite differentiation indicate a mature arc and thickened crust during the advanced stage of the evolution of Neoarchean Bundelkhand greenstone belt in a convergent tectonic setting where the melts were derived from partial melting of thick basaltic crust metamorphosed to amphibolite-eclogite facies. The trace element systematics suggest the presence of arc-back arc association with varying magnitudes of crust-mantle interaction. La/Sm, La/Ta, Nb/Th, high MgO contents (>20 wt.%), CaO/Al_2O_3 and $(Gd/Yb)_N > 1$ along with the positive Nb anomalies of the komatiite basalts reflect a mantle plume source for their origin contaminated by subduction-metasomatized mantle lithosphere. The overall geochemical signatures of the ultramafic-mafic and felsic volcanic rocks endorse the Neoarchean plume-arc accretion tectonics in the Bundelkhand greenstone belt.

1. Introduction

Archean greenstone belts present in different cratons comprising wide variety of volcano-sedimentary rocks recording various tectonic imprints and evolutionary history, intrusive and extrusive magmatic episodes, metamorphism, metasomatism and

* Corresponding author. Geochemistry Division, CSIR-National Geophysical Research Institute, Uppal Road, Hyderabad, Telangana, 500007, India.
E-mail address: cmaningri@gmail.com (C. Manikyamba).
Peer-review under responsibility of China University of Geosciences (Beijing).

https://doi.org/10.1016/j.gsf.2017.08.008

mineralization (Weaver and Tarney, 1981; Pearce, 2014). Based on geological, geophysical, geochemical and geochronological investigations, several studies have suggested that Phanerozoic type plate tectonics were operative in the Archean era and correlated these with the modern-style convergent margin processes (Condie, 2000; Benn et al., 2006; Furnes et al., 2014; Santosh et al., 2016; Yang et al., 2016; Yang and Santosh, 2017). A peak in continental crustal growth at 2.7 Ga, existence of hotter Archean mantle, eruption of komatiites, occurrence of tonalite–trondhjemite–granodiorite (TTG) and adakites that are geochemically analogous to their Phanerozoic counterparts lend support to the operation of plate tectonics during Archean including both mantle plume and island arc processes (Isley and Abbott, 1999; Kerrich and Polat, 2006; Polat and Kerrich, 2006 and references there in). Convergent margins act as magma producing centres through partial melting in the mantle wedge and subducted oceanic slab representing important sites of crustal growth in both Precambrian and Phanerozoic Eras (Taylor and McLennan, 1985; Rudnick, 1995; Tatsumi, 2005; Stern and Johnson, 2010; Xiao and Santosh, 2014; Santosh et al., 2015, 2017). Intraoceanic arc lithologies such as boninites, low-Ti tholeiites, picrites, high magnesian andesites, and Nb-enriched basalts from greenstone belts of different Archean cratons and their Phanerozoic counterparts provide clue to understand convergent margin tectonics and crustal growth (Manikyamba et al., 2004, 2005, 2009, 2012, 2015a,b; Manikyamba and Khanna, 2007; Manikyamba and Kerrich, 2012; Baitsch-Ghirardello et al., 2014). The lithological assemblages of the Neoarchean greenstone belts from different cratons of the world preserve distinct geological and geochemical signatures of subduction processes (Hollings and Kerrich, 2000; Smithies et al., 2005; Polat and Kerrich, 2006; Zhai and Santosh, 2011; Shchipansky et al., 2012; De Joux et al., 2014; Furnes et al., 2014; Santosh et al., 2016).

The Bundelkhand Craton is one of the prominent Archean nuclei in the northern part of the Indian shield across the north of Son–Narmada lineament (Fig. 1). Paleoarchean TTGs, Mesoarchean gneisses of 3551–3270 Ma (Mondal et al., 1998, 2002; Kaur et al., 2014) and Neoarchean granitoids of 2583–2516 Ma (Mondal et al., 2002; Kumar et al., 2010; Pandey et al., 2011; Joshi et al., 2013; Kaur et al., 2016; Saha et al., 2016) are extensively exposed covering an area >30,000 km^2 (Fig. 1A and B).

Previous studies have reported supracrustal rocks of greenstone and associated magmatic suites in the Bundelkhand Craton (Malviya et al., 2006; Singh et al., 2007; Singh, 2012; Singh and Slabunov, 2015, 2016; Kaur et al., 2016; Saha et al., 2016). However, detailed petrological and geochemical studies on the mafic-ultramafic-felsic sequences documenting their tectonic setting along with the style and nature of magmatism are very limited on Mauranipur-Babina greenstone belt. In this paper, we document systematic geological, petrological and geochemical studies on different lithologies of various Formations occurring at Mauranipur, Babina-Dhaura and Umari sections of the central part of Bundelkhand Craton to evaluate their geodynamic setting.

2. Geological setting

The Bundelkhand Craton is bound by the NE–SW trending Great Boundary Fault in the west, ENE–WSW trending Son Narmada Faults in the south and NW–SE trending Yamuna Fault from Indo-Gangetic alluvium in the north (Bhattacharya and Singh, 2013) consisting of Mesoarchean to Paleoproterozoic lithologies (Mondal et al., 2002; Kumar et al., 2011; Mohan et al., 2012 and references there in). The craton is semi-circular in shape and occupies an area of about 30,000 km^2 in north-central part of the Indian shield (Basu, 1986; Fig. 1A and B). It is overlain in the east, west and south by the Meso–Neoproterozoic sedimentary rocks of Vindhyan Supergroup (Ray, 2006) and in the south-east and south by Paleoproterozoic Bijawar Group (Pandey et al., 2011) comprising low grade volcano-sedimentary rocks. The south-western fringe is demarcated by a small outcrop of the Deccan basalt and the northern part is hidden under the recent alluvium of Indo-Gangetic Plains (Singh et al., 2007). The Bundelkhand massif is mainly composed of (1) Mesoarchean Bundelkhand Gneissic Complex (BnGC) with tonalite–trondhjemite–granodiorites (TTG); (2) Neoarchean greenstone sequences consisting a variety of volcano-sedimentary rocks; (3) subsequent granites intruded into the greenstone belt sequences marks a major geological event for the cratonization and (4) Proterozoic quartz reefs and mafic dykes emplaced subsequent to transformation into a stable craton that are related to crustal scale extension and shearing (Basu, 1986; Rao et al., 2005; Pati et al., 2007; Singh, 2012; Bhattacharya and Singh, 2013).

The Neoarchean Bundelkhand granitoids occur extensively over a large part of the Bundelkhand Craton (>70% of the area), intrude the greenstone sequences and high grade (amphibolite-granulite facies) metamorphic (Singh et al., 2007). The Neoarchean felsic magmatism (2532–2516 Ma; Mondal et al., 2002; Kumar et al., 2010; Saha et al., 2011; Joshi et al., 2013; Singh and Slabunov, 2015) is considered to mark the final stabilization of the craton (Ray et al., 2015). This belt is about 120 km long and 6–7 km wide, and carries E–W trending disseminated linear bodies in the central part of the craton (Mohan et al., 2012; Singh, 2012; Ray et al., 2015; Singh and Slabunov, 2015; Fig. 1B). The E–W trending greenstone belt has extensive outcrops at Umari-Bhauti (near Mohar), Babina-Dhaura (Fig. 1C) and Baragaon-Mauranipur (Fig. 1D) areas and is dismembered by younger granites and quartz reefs. The greenstone belt is easily distinguished from rocks of BnGC by their grade of metamorphism, lithological associations, texture, structures and presence of sheared angular relationship with Bundelkhand gneisses (Singh et al., 2007). The metamorphic P-T conditions as derived from the garnet-sillimanite ± biotite ± cordierite-feldspar-quartz and garnet-biotite-amphibole-plagioclase-quartz assemblages of gneisses (BnGC), range from 4.9 to 6.4 kbar and 680 to 730 °C (Singh and Dwivedi, 2009), suggesting amphibolite to granulite facies (Singh and Dwivedi, 2015). The presence of mineral assemblages such as garnet-chlorite-biotite-K-feldspar-quartz in pelitic rocks and cummingtonite ± grunerite-magnetite-chlorite ± biotite-quartz in BIF and talc-chlorite-actinolite-tremolite ± quartz in metabasalts, and their P-T estimates of 500 ± 50 °C temperature and 4–5 kbar pressure (Singh, 2012) suggest low grade metamorphic conditions in the greenstone belt.

2.1. Bundelkhand greenstone belt

The E–W trending greenstone belt in the central part of the craton (Sharma, 2000; Malviya et al., 2006; Singh et al., 2007) has been divided in to four Formations based on lithological characters, structural and field relationships (Table 1; Fig. 2). The Baragaon Formation is the lowermost unit of this belt and the rocks of this Formation are mainly confined to east of Mauranipur town (Table 1; Fig. 2). The E–W trending Bundelkhand greenstone belt show angular relationship with the BnGC. The gneissic rocks are rotated to E–W towards the contact (Singh et al., 2007). The pink granite shows intrusive relations and is undeformed. A NE–SW trending quartz reef shows sinistral displacement of the metamorphic units of the greenstone belt and the BnGC at Mankua locality. The Baragaon Formation is represented by a variety of ultramafic-mafic extrusive and intrusive rocks (Fig. 3a,c) in the lower part and Mg enriched andesite (Fig. 3d), basalt and dacite in the upper part (Singh, 2012). Several peridotite and gabbro dykes intrude into the

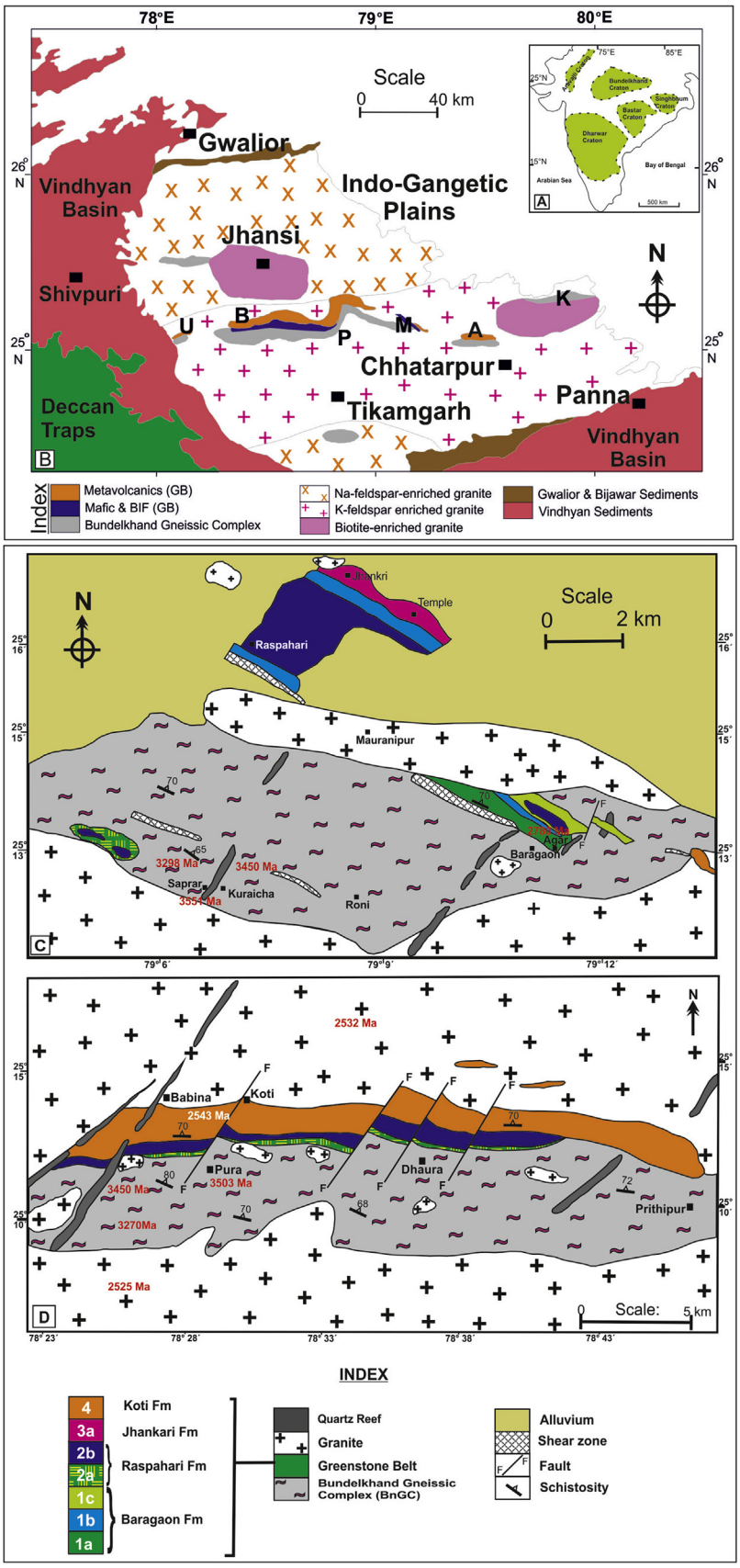

Figure 1. (A) Inset map showing the major cratons of India (after Sharma, 2009), (B) regional geological map of Bundelkhand craton showing Bundelkhand Gneissic Complex (BnGC) and E–W trending greenstone belt in the central part of the craton (modified after Singh et al., 2007; U–Umari; B–Babina; P–Prithipur; M–Mauranipur; A–Ajnar and K–Kabarai), (C) geological map shows various litho units of greenstone belt at Mauranipur and (D) represents the geological map of Babina-Dhaura section where the greenstone belt is truncated by different faults and shears.

Table 1
Tectonostratigraphic elements of the greenstone belts, Bundelkhand craton.

Mauranipur section (age in Ma)	Babina-Dhaura section (age in Ma)	Umari-Bhauti section	Major lithologies	Minor lithologies	Volcanic/sedimentary/ metamorphic structures	Intrusive units	Metamorphic grade/ facies	Tectonic structures	Structural trend
–	–	Bhauti Fm.	(3b) Carbonates, siltstone quartzite, C-shale, phyllite	andesite, chert, calc schists	Stromatolite type structure, ripple marks, graded beds	Basic dykes, granites	Greenschist facies	F1-F2; F3 S1-S2	E–W, NE–SW
Jhankari Formation (3a)	–	–	(3a) Quartzite, Graywackes, phyllite and chlorite schist	Micaceous quartzite, fuchsite quartzite, tuffacious greywacke	Cross bedding, Graded bedding	Mafic dykes, Granites	Lower greenschist facies	F1-F2; S1	NNW–SSE/ ENE–WSW
–	Koti Fm. (2542 ± 17 Ma)	Umari Fm.	(4a) Rhyodacite, andesite, dacite, rhyolites (4b) Agglomerates, rhyolites and tuffs	agglomerate, massive basalts (rare), mylonites tuffacious cherts	Felsic flows, tuffacious structures Vertical shears and mylonites	Pink granite, Mafic dykes	Mylonitised and lower greenschist facies	F1-F2; S1-S2	E–W, NE–SW
Raspahari-Dhaura Formation	Dhaura Fm.	–	(2a) Mafics and ultramafics (2b) Banded magnetite quartzite, basalt, cherts, quartzite	tuffs, basic volcanics intercalated with BMQ, ultramafic dyke sheets	Penecontemporaneous deformational structure in BMQ	Pink granite and mafic dykes	Greenschist to lower amphibolites facies	F1; S1 F1-F2 S1-S2 Open folds	E–W, NE–SW
Baragaon Formation (2750 ± 8 Ma)	Pura Fm.		(1a) Basalts (pillow & massive) (1b) komatiite basalt, peridotite (1c) Felsic volcanics, andesites & dacite (1d) grabboic dykes (1e) K_2O enriched basalt and tuffs	Mg-andesite, dacite, volcanogenic/ chemogenic sediments quartzite, sepentinised peridotite, asbestos sheets chl schist, talc schist, mafic and ultramafic flows	Pillows and amagdular basalts, flow structures in andesites	Gabbroic dyke, quartz reefs	Greenschist facies	F1-F2 F3 S1-S2 Mostly open folds	WNW–ESE, NE–SW
Bundelkhand gneissic complex (3200–3300 Ma)			Gt – crd gneisses, Gt sill gneisses, gt – bt gneisses, granite gneisses migmatites and TTGs	Quartzites, amphibolites, gt-amphibolites	Gneissose and granulose structures	TTGs invade the pelitic gneisses	Upper amphibolite to granulite facies	Hook folds sheeth fold, tight folds	NW–SE, NE–SW and E–W

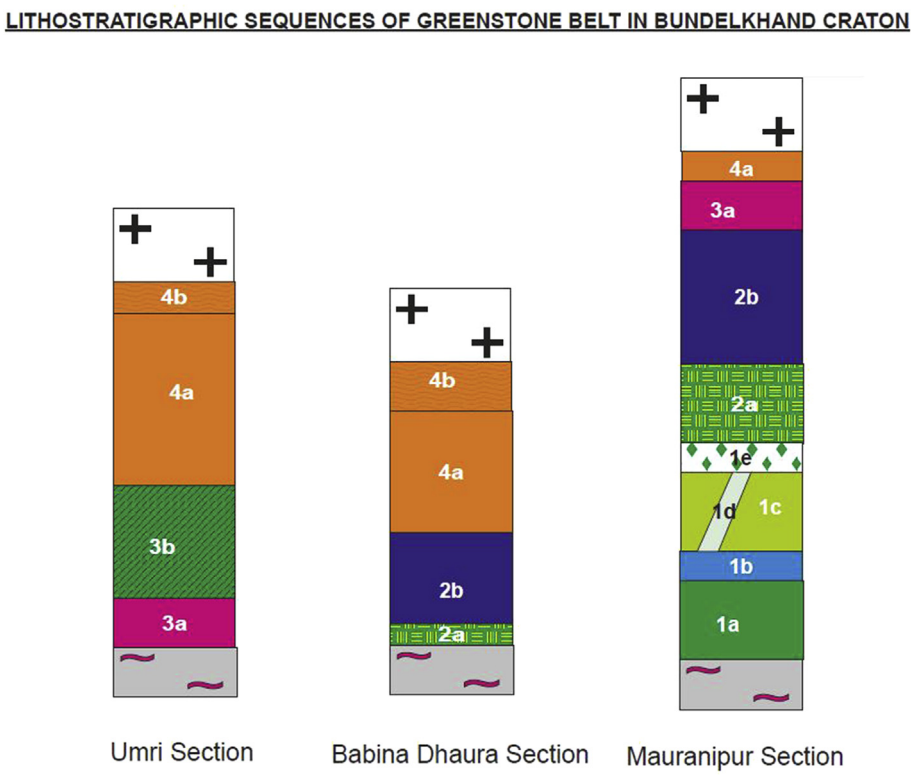

Figure 2. Field relationship and correlations of different litho units of various Formations of greenstone belt of Bundelkhand which are exposed at Umri in west, Babina–Dhaura central part and Mauranipur in the east located in the Bundelkhand Craton represented by U, B and M in Fig. 1B. The legend and symbols are similar as shown in Fig. 1.

middle and upper parts. Several exotic blocks of mafic and ultramafic rocks along with the metamorphic units have also been recorded in this study from the upper part. The Raspahari Formation comprises mainly clastic and non-clastic volcanogenic sediments (Fig. 3b) and minor amount of basic volcanics at some places (Prasad et al., 1999; Singh et al., 2007). Unlike the Baragaon Fm., thinly bedded rocks of BIF (Fig. 3b) occur throughout the greenstone belt in the form of long linear ridges confining to small mounds. Thick intercalated bands of magnetite-quartzites (up to 30 cm in thickness of magnetite) were recorded from east of Baragaon village in the eastern part of greenstone belt where this Formation has acquired the maximum thickness and extension. Tuffs with metabasic lenses, lenticular bodies of magnetite, quartzite, cherts and basic flows are also noted from the thick sequences of banded iron formation (BMQ) at Babina and Mauranipur areas (Singh, 2012). The lower part of this Formation is characterized by 3 to 4 m thick basaltic flows with minor ultramafics (Fig. 3c,d) followed by BIF and micaceous quartzites. The Umari–Jhankari Formation is represented by thick succession of arkose-argillite-carbonate sequence with very rare occurrence of volcanic flows in the western part of greenstone belt (Pandey et al., 2011). The graded bedding, ripple marks and current bedding structures have been recorded from the Bhauti area. The upper part of this sequence also occurs at Jhankari and Swargashram temple in the north of Mauranipur located in the eastern portion of greenstone where this is dominated by metapelites, sandstone, micaceous quartzite, greywacke and fuchsite quartzite (Sharma, 2000; Singh, 2012). The mafic lavas are very rare in this Formation. These rocks are highly deformed and metamorphosed into greenschist facies and are intruded by coarse grained granite. The Koti Fm. is the upper most sequence of Bundelkhand greenstone sequence that represents the felsic volcanism consisting of rhyolite, rhyodacite, dacite (Fig. 3e and f), granite breccias, agglomerates, felsic dykes and andesite (Prasad et al., 1999; Singh et al., 2007). The basaltic lava occurs occasionally in this Formation. The rocks of this formation are observed throughout the greenstone belt. The presence of felsic dykes and thick shear zones are also noted in the Koti Fm. The greyish pink variety of felsic volcanics are dominant in the western part, whereas pinkish and chocolate coloured rhyolites and rhyodacites occur in the eastern part of the greenstone belt. The medium to coarse grained K-rich pink granite demarcates the end of the evolution of greenstone belt in the central part of craton (Singh et al., 2007; Singh, 2012).

Geochronological data on this greenstone belt associated with the Bundelkhand gneisses is very scanty. The pink granite and granodiorite which intrudes the greenstone sequence have been dated as 2581 to 2516 Ma (Mondal et al., 2002; Kumar et al., 2011; Pandey et al., 2011; Joshi et al., 2013; Kaur et al., 2016). The Mesoarchean Bundelkhand gneiss is older than the associated greenstone belt (3551–3270 Ma; Sarkar et al., 1996; Mondal et al., 2002; Kaur et al., 2014; Saha et al., 2016). The felsic volcanic rocks of Koti Fm. from Babina and Bhauti areas are dated at 2542 and 2622 Ma (U-Pb and Pb-Pb whole rock; Pandey et al., 2011; Singh and Slabunov, 2015, 2016). The only available date for the crystallization age of the basaltic rock of Baragaon Formation shows 2780 Ma (Slabunov et al., 2013). On the basis of the available geochronological data it is suggested that the Bundelkhand greenstone belt comprising Baragaon, Raspahari, Umari-Jhankari and Koti Formations (Table 1; Fig. 2) which were initiated ~2780 Ma with ultramafic-mafic magmatism and culminated around 2542 Ma with extensive felsic volcanism. The present study deals with extrusive and intrusive rocks of ultramafic, mafic and felsic volcanic rocks in which the basalts have been classified as type I (pillow lavas associated with ultramafic rocks), II (massive and associated with BIF) and III (massive and associated with felsic rocks) based on their field and geochemical characteristics.

Figure 3. Field photographs showing different structures in the Bundelkhand greenstone belt (a) pillow structures (type I Basalt) showing deformation and alteration from Baragaon Fm., (b) oxide and sulphide facies banded magnetite –quartzite (BMQ) from Raspahari Fm., of Mauranipur (c) massive type II basalt from Kuraicha village (d) andesite from the upper part of Baragaon Fm., (e) massive rhyodacite from Koti Fm. of Babina and (f) vertical shearing in the felsic volcanic rocks of Koti Fm. at Babina.

2.2. Structure

The greenstone belt represents a syncline and trends NW–SE, traversed by Neoproterozoic granitoids at Mauranipur. The pink granite intrudes into the metavolcanics and gneisses (Fig. 1C) where the rocks occurring to the north of Mauranipur (Jhankari and Raspahari Formations) display southward dip and those to the south of Mauranipur at Baragaon, north of Saprar and Baragaon Formation at Agar village, are inclined towards north (Fig. 2a). Bedding as a planar structure observed in banded magnetite-quartzite (BMQ), fuchsite quartzite and greywacke are marked by compositional layering and colour bands (Fig. 3b). The thickness of BIF varies from few millimetres to centimetres. These rocks trend ENE to WSW direction with 60°–70° northerly dips. The low-grade metamorphosed BIF of Saprar section (south of Mauranipur) exhibits crenulation cleavages (Fig. 3d). The fold axes trend NW to NE with 30°–40° plunge. A series of ENE–WSW trending open folds, and sometimes overturned isoclinals folds, have been recorded form BIF (Singh et al., 2007). The E–W trending vertical crustal-scale shears are prominent in these two areas (Fig. 3f). The metavolcanic rocks of Koti Formation at Babina are characterized by E–W trending vertical shears where coarse grained granite cut across the vertical shear planes (Fig. 3f). These shears are ductile to brittle-ductile in nature, and are more or less parallel to the strike of the greenstone belt (Singh and Bhattacharya, 2010). The entire E–W trending greenstone belt is subsequently truncated by the NE–SW trending quartz reefs and crustal scale shears, and sometimes dislocated by local faults that passes through the greenstone belt (Fig. 1C and D). As a result, the rocks of the greenstone belt are displaced about 1.0–1.5 km at few places (Basu, 1986; Bhattacharya and Singh, 2013). In addition to the E–W and NW–SW trending crustal scale shear zones, a series of N–S trending conjugate type crustal scale shears also passes through metavolcanics of the Koti Formation at Babina and Dhaura areas. Thus, the NW–SE, NE–SW and N–S trending crustal scale shears (Singh and Bhattacharya, 2017) indicate the influence of post evolution structures in the greenstone belt.

3. Petrographic characteristics

The intrusive and extrusive ultramafic rocks show alteration including saussuritization and uralitization effects. Altered minerals such as serpentine, chlorite, secondary amphiboles and opaques are present within the fine grained groundmass of plagioclase and clinopyroxene in pillow basalt of Mauranipur. The pseudomorph of olivine grains are occasionally observed with abundant talc and tremolite in komatite basalt. Similar texture was also reported by Malviya et al. (2006) from ultramafic of Baragaon. In the intrusive variety, the amphiboles are coarse grained. Disseminated granules of chromite are also present. The type-I basalt shows poorly developed foliation imparted by the actinolite and chlorite (Fig. 4a). The other mineral constituents include plagioclase (oligoclase), magnetite, quartz and epidote. Occasionally, relicts of olivine and pyroxene are also observed. Type-II basalts are more deformed and metamorphosed compared to type I and are characterized by medium grained chlorite, tremolite and actinolite minerals aligned along the schistose plane (Fig. 4b). These rocks in general exhibit schistose textures and rarely exhibit subophitic texture. Amphibole-bearing pyroxenite occurs as thrust sheet at the base of BIF at Pura village (Babina section), which is characterized by cumulate texture. The coarse grained epidote, actinolite, flakes of chlorite are common as altered minerals. The plagioclase and pyroxene are deformed and sometimes showing rotation texture (Fig. 4c). The ultramafic rocks at Swargeswar Ashram (marked as "Temple" in Fig. 1C), are characterized by coarse grained pyroxene with relicts of plagioclase and olivine. Malviya et al. (2006) described them as komatiite basalts. The Mg-andesites and dacites at Mauranipur are less deformed and metamorphosed than pillow basalts and are characterized by frequent occurrences of secondary epidote and actinolite (Fig. 4d). Phenocrysts of plagioclase and hornblende are common in the Mg-andesite.

The meta-rhyolite and rhyodacites of Koti Formation show flow bands imparted by oriented alignment of K-feldspar, quartz and rarely plagioclase (Fig. 4e). The accessory minerals include chlorite, magnetite and epidote (rare) which are alteration products. Occasionally, phenocrysts of hornblende constitute part of the flow banding. The rhyodacite is less deformed and metamorphosed compared to the rhyolite and is characterized by fine to medium grained hornblende, chlorite and actinolite (Fig. 4f). The phenocrysts of plagioclase and hornblende are abundant in the rhyodacite compared to the rhyolite.

4. Analytical methods

Sixty samples representing the major lithologies described in the previous section were selected from Baragaon, Mauranipur, Koti, Saprar (Kuraichha), Babina, Bhauti and Dhaura from east to west within the Bundelkhand greenstone belt. Major and minor oxide determinations were carried out using XRF technique (Krishna et al., 2007) and whole rock trace, REE concentrations are estimated using HR-ICPMS at CSIR-NGRI, Hyderabad, following the standard methods of sample decomposition techniques and methods of analysis, instrument parameters and precision are referred to Subramanyam et al. (2013) and Manikyamba et al. (2015a,b). The certified reference materials such as UB-N, BHVO-1, JB-2, JA-2 and JR-1 (United States Geological Survey and Geological Survey of Japan) have been used as matrix matching standards for trace and REE analysis. The precision, accuracy and Relative standard deviation (RSD) are given in Manikyamba et al. (2014c, 2015b) and Rajanikanta Singh et al. (2017).

5. Results

5.1. Ultramafic unit

5.1.1. Komatiitic basalt (KB)

The MgO enriched variety (>20 wt.%) has low-Cr contents with olivine adcumulates, whereas low MgO variety of KB (<20 wt.%) is saturated in Cr contents and low content of orthocumulates of olivine. The Mg# varies between 81 and 86. Arndt and Lesher (2004); Arndt and Nisbet (1982) suggested that the term komatiitic basalt can be applied to volcanic rocks containing less than 18 wt.% MgO that can be linked, using petrological, textural or geochemical arguments, to komatiites. Further, they also argued that the MgO content varies from 18% to 50%, the limit between komatiitic basalt and komatiite, due to olivine fractionation or accumulation in low-viscosity ultrabasic liquids. Komatiite basalts have been reported from various stratigraphic sequences of greenstone belts (Arndt and Nisbet, 1982; Rollinson, 1999; Jayananda et al., 2013; Manikyamba et al., 2013) and described as high- and low-Mg type komatiite basalts (Sproule et al., 2002). In the present work, the ultramafic volcanics showing MgO contents are well above 18 wt.% (Supplementary Table 1). Hence, the term "komatiitic basalt" is used in conjunction with other geochemical properties. In figure legends komatiite-1 and 2 are used to differentiate the intrusive komatiite basalt (amphibole bearing pyroxenite) and extrusive komatiite basalt respectively. The komatiite basalt flows (extrusive) and cumulates (intrusive) of present study area show very narrow range of MgO (22–25 wt.%) and a wide variation in Cr content (3100–14,290 ppm in cumulates;

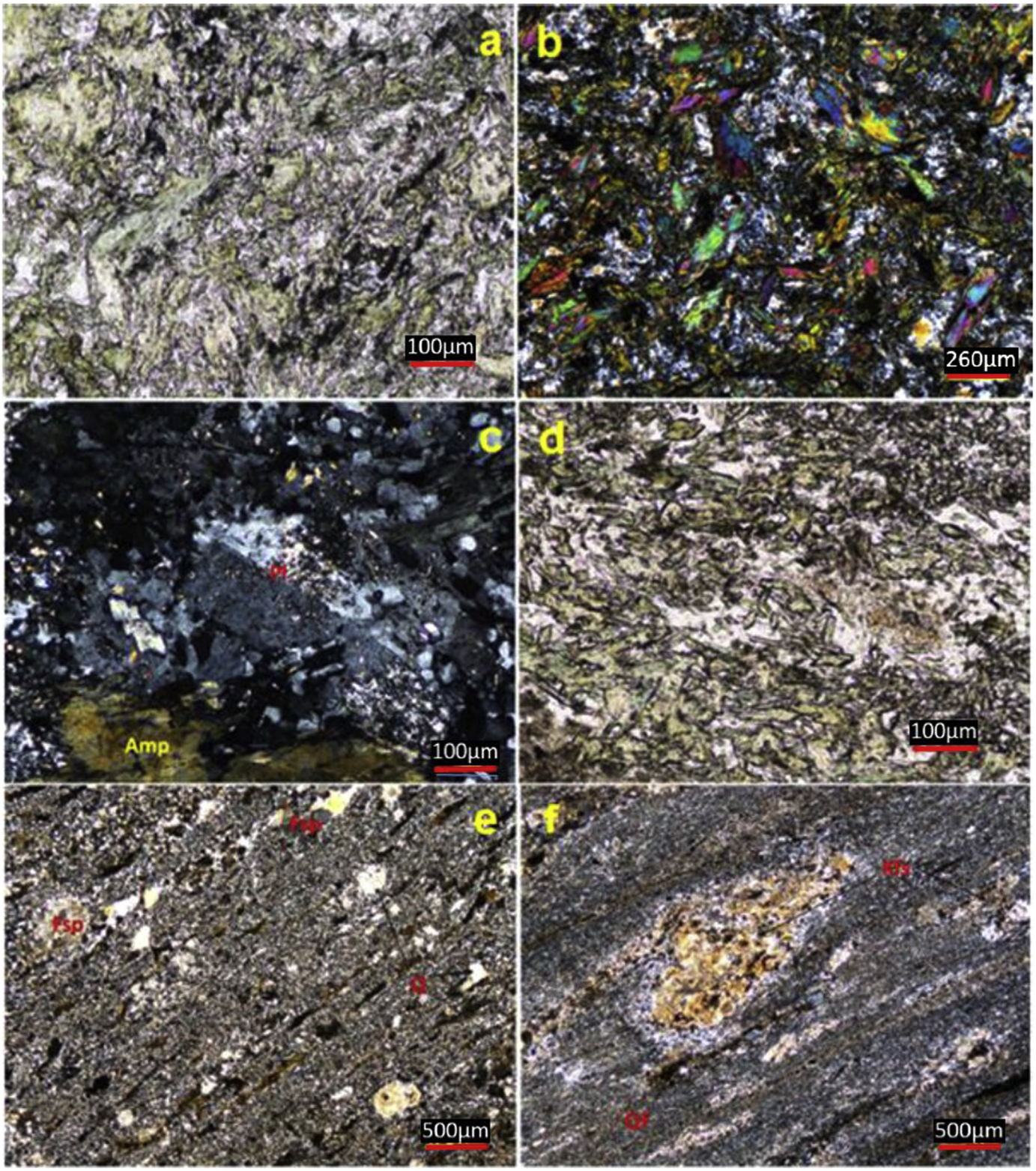

Figure 4. Photomicrographs of (a) Type - I basalt showing mild foliation defined by the presence of chlorite and elongated epidote, (b) development of chlorite and actinolite in type – I where coarse grained magnetite and relics of augite is present, (c) coarse grained cumulates of amphibole and pyroxene from ultramafic intrusive at Babina, (d) alteration and deformation texture in Mg-andesite showing needle shaped amphiboles and epidotes from the upper part of Baragaon Fm., (e) Rhyodacite showing banded structure represented by amphiboles and plagioclase from Babina and (f) bands and flow texture in metarhyolite of Koti Fm. at Babina.

292–846 ppm in flows), indicating depleted to enriched mantle (heterogeneous mantle) conditions. The komatiite basalts of present study correspond to tholeiitic trend with Mg enrichment (Fig. 5a; Irvine and Baragar, 1971).

On Nb/Y vs. $Zr/TiO_2 \times 0.0001$ diagram (Fig. 5b), the studied samples plot in the field of sub-alkaline basalts with very low to moderate Zr/TiO_2 ratios. The MgO relationship with different major elements and Ni shows that the analyzed samples plot below the olivine control line for SiO_2, Fe_2O_3 and Ni and above olivine control line for Al_2O_3, TiO_2 and P_2O_5. The komatiite basalts (MgO >20 wt.%; TiO_2 >0.5 wt.%) with low $(Gd/Yb)_N < 1$ and high $(Gd/Yb)_N > 1$ contents are related to cumulates and flows respectively (Rollinson, 1999; Manikyamba et al., 2013) and is related to presence of garnet in the melt source.

5.1.2. Amphibole-bearing pyroxenite (cumulate ultramafic intrusives)

The SiO_2, TiO_2, MgO and Fe_2O_3 contents of intrusive ultramafic rocks are characterized by minor variations in their major elements with Mg# varying from 53 to 78 suggesting the depleted nature of the melts (Supplementary Table 1). These samples correspond to tholeiitic trend with Mg enrichment (Fig. 5a; Irvine and Baragar, 1971). On Nb/Y vs. $Zr/TiO_2 \times 0.0001$ discrimination diagram (Fig. 5b), the studied samples plot in the field of sub-alkaline basalts. MgO relationship with different major elements and Ni, exhibit a cluster over a narrow range of MgO (except 2 samples) and plot below and above the olivine control line for SiO_2, Fe_2O_3 and Ni and Al_2O_3, TiO_2 and P_2O_5 respectively. These rocks are characterized by moderate Ni (197–463 ppm), Co (43–79 ppm) and Cr (292–847 ppm) contents. Except Nb (10.4–25.6 ppm) and Zr (8.75–24.54 ppm), the large ion lithophile elements (LILE) show relatively lower concentrations (Rb = 6–126 ppm; Sr = 5.49–14.27 ppm; Ba = 47–85 ppm) compared to high field strength elements (HFSE) such as Ta (0.01–0.06 ppm), Hf (0.38–0.98 ppm), Th (0.44–1.25 ppm) and U (0.02–0.14 ppm). The studied samples are characterized by enriched LREE $[(La/Sm)_N = 2.18–2.98]$, flat HREE patterns $[(Gd/Yb)_N = 0.40–0.45]$ and significant negative Eu anomalies (Fig. 6). Primitive mantle normalized multi-element diagram (Figs. 6 and 7) shows a progressive enrichment from Th to Yb, with positive Nb, Hf, Ti and Y anomalies.

5.2. Mafic unit

The SiO_2 content of the analyzed samples vary from 44.7 to 53.6 wt.% and plot in the field of sub-alkaline basalts and andesite/basalt in Nb/Y vs. Zr/TiO_2 binary diagram (Fig. 5b; Winchester and Floyd, 1977) and exhibit sub-alkaline tholeiitic to transitional affinity (Ross and Bedard, 2009; Fig. 4c; Supplementary Table 1). Their Mg# varying from 37 to 73. MgO relationship with selected major oxides depicts magmatic trends. Type-I basalts have $\sum$REE = 32.41–53.87 ppm and display flat chondrite normalized LREE patterns (Fig. 6) with weak or no negative Eu anomalies, $(La/Sm)_N = 1.22–1.48$, $(Gd/Yb)_N = 1.02–1.28$ and $(La/Yb)_N = 1.13–1.66$, whereas the type-II basalts have $\sum$REE = 10.9–90.44 ppm and display flat chondrite normalized LREE patterns (Fig. 6) marked by weak positive and negative Eu anomalies, $(La/Sm)_N = 0.67–1.65$, $(Gd/Yb)_N = 1.04–1.73$; $(La/Yb)_N = 0.6–3.4$ and Zr/Nb = 6.5–16.8.

Primitive mantle-normalized multi-element patterns (Fig. 6) show significant negative anomalies of Nb, Zr, Hf and Ti for Type-II basalts, while Type-I basalts have insignificant Zr and Hf anomalies. The type III basalts are geochemically distinct with higher TiO_2 contents (1.97–2.04 wt.%) compared to Type I and II varieties, lower $\sum$REE (88–90 ppm) compared to type I basalts and display slightly enriched LREE patterns $[(La/Sm)_N = 1.50–1.59$; $(Gd/Yb)_N = 1.69–1.68$; $(La/Yb)_N = 3.2–3.4]$ with flat HREE and without any Eu anomalies (Fig. 6). Primitive mantle-normalized multi-element patterns (Fig. 6) show distinct LILE and slight HFSE enrichment and exhibit near flat trend for Zr, Y and Yb. Thus, these three types of basalts of the Bundelkhand greenstone belt from different stratigraphic sequences are characterized by distinct geochemical characteristics showing Nb, Zr, Hf, Ti and Hf negative anomalies (Type-I and Type-II basalts) and a very smooth to near flat trend of Zr, Y and Yb (Type III).

5.3. Intermediate unit (andesite–dacite and Mg-andesite)

The intermediate unit from the upper part of Baragaon Formation shows SiO_2 values ranging from 53.3 wt.% to 64.5 wt.% and classified as andesites (Fig. 4b) in which majority of the samples indicate calc-alkaline trend, while four of them plot in tholeiitic field (Fig. 4a; Irvine and Baragar, 1971; Supplementary Table 1). Their Mg# varies between 42 and 74, indicating their high Mg-contents. These samples possess similar HFSE and REE contents and inter-element ratios as Type-I basalts, however, there is slight enrichment in LREE compared to Type-I basalts probably reflect their fractionation from the basaltic magma. The higher SiO_2 of andesites relative to Type-I basalts is accompanied by greater Th, La and $(La/Sm)_N$. These samples display LREE enriched chondrite normalized REE patterns (Fig. 7A) with weak negative Eu anomalies $(La/Sm)_N = 2.46–3.42$, $(Gd/Yb)_N = 0.82–1.50$ and $(La/Yb)_N = 3.14–6.55$.

5.4. Felsic unit (rhyolite-rhyodacite-dacite)

The felsic rocks associated with the type III basalts of the Koti Formation are characterized by high SiO_2 (64.6–66.6 wt.%), low TiO_2 (0.4–0.6 wt.%), MgO (1.9–3.1 wt.%), Cr (5–13 ppm) and Ni (1–2 ppm) contents (Supplementary Table 1). Their Mg# varies between 54 and 59. In terms of immobile trace element relationships (Fig. 4b), the analyzed rocks exhibit rhyolitic characteristics with distinct alkaline nature (Fig. 4b; Irvine and Baragar, 1971). The REE and primitive mantle-normalized diagrams (Fig. 7C) shows coherent LREE enriched patterns marked by weak negative Eu anomalies $((La/Sm)_N = 1.61–5.57$, $(Gd/Yb)_N = 1.11–1.97$ and $(La/Yb)_N = 2.20–17.10)$; pronounced negative Nb and positive Ti anomalies; variable negative to positive Zr anomalies, likely due to zircon fractionation or accumulation.

6. Discussion

6.1. Alteration and crustal contamination

Numerous studies on Archean volcanic rocks have shown that metamorphism and alteration are capable of mobilizing elements and resetting isotopic compositions (Lahaye and Arndt, 1996; Lesher et al., 1997; Polat et al., 2002; Ordóñez-Calderón et al., 2008). High field strength elements (HFSE: Th, Nb, Ta, HREE, Y, Zr and Hf) and transition elements (Cr, V, Sc, Ti, Mn, Fe, Mg, Co and Ni) present within the igneous phases (olivine, pyroxene, chromite) or accommodated in metamorphic minerals (amphibole and chlorite) retain their original geochemical distribution of the rocks even they are subjected to alteration. The large-ion lithophile elements (LILE: Cs, Rb, K, Na, Sr, Ba, Ca and Eu^{2+}), are not accommodated in metamorphic minerals, but are concentrated in the readily-altered glass phase and are commonly mobile (Lahaye and Arndt, 1996; Lesher and Stone, 1996; O'Hanley, 1997). Studies indicate that Ce anomalies occur in response to oxidation of Ce^{3+} to Ce^{4+} from solution as CeO_2 (Braun et al., 1993). Ce/Ce* ratios between 0.9 and 1.1 display limited LREE mobility whereas those with Ce/Ce* <0.9 and >1.1 are characterized by large LREE mobility (Polat et al., 2002).

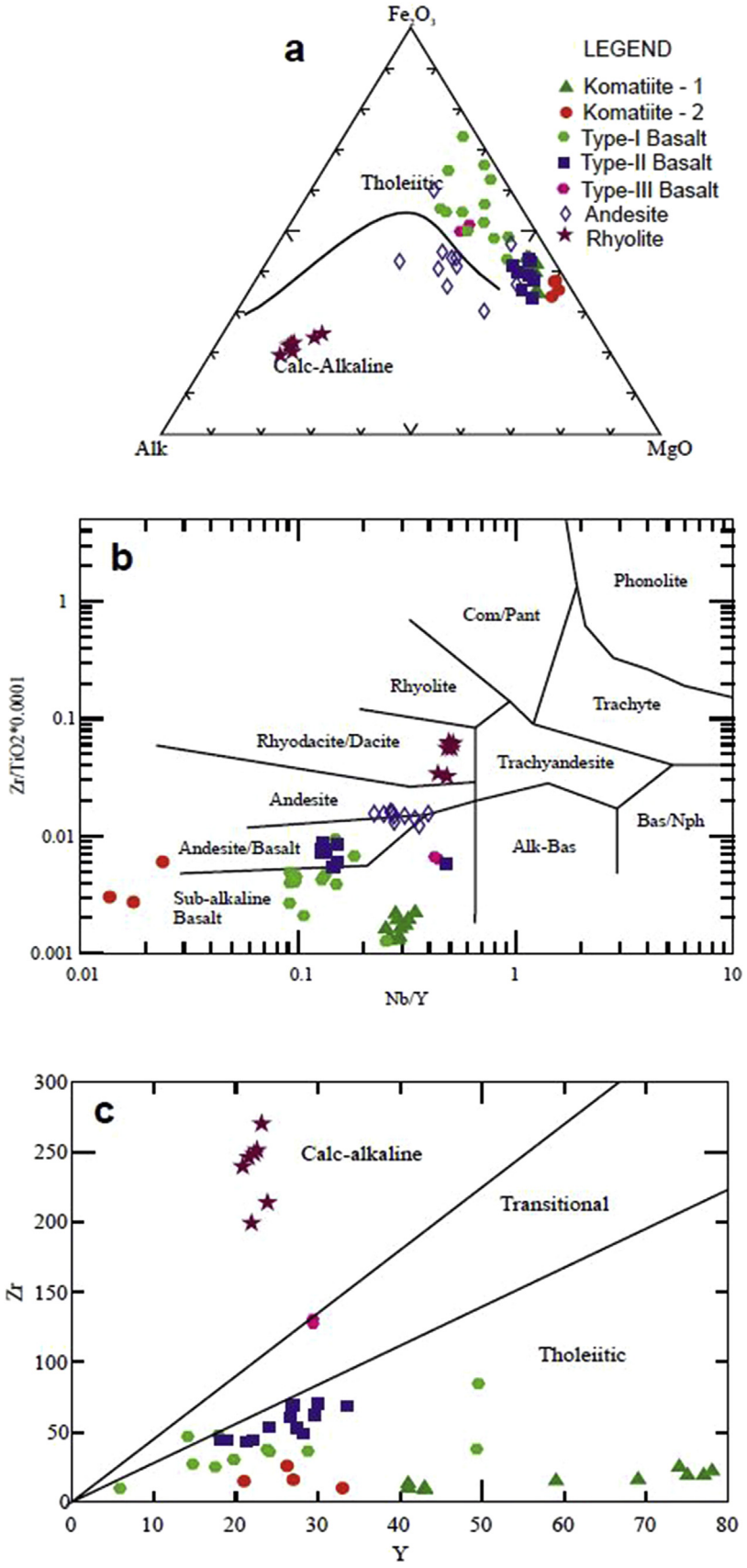

Figure 5. (a) AFM diagram of Irvine and Baragar (1971) showing calc-alkaline nature of andesites and rhyolites and komatiic basalts and basalts in tholeiitic field (b) Nb/Y vs. Zr/TiO_2 diagram (after Winchester and Floyd, 1977) showing variation from sub-alkaline basalts to dacites (c) Zr vs. Y plot (in ppm) of Ross and Bedard (2009) indicating the tholeiitic nature of these rocks.

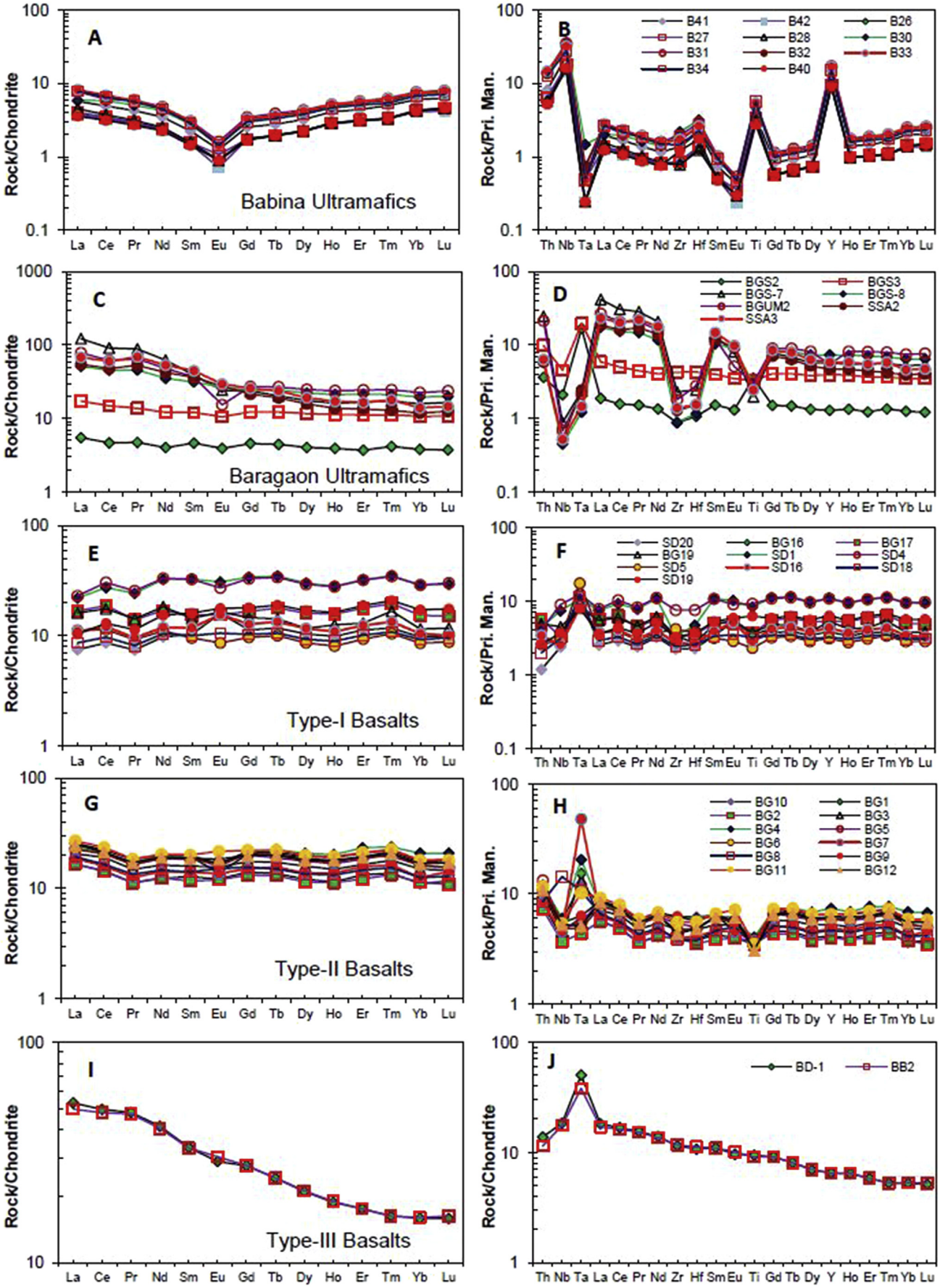

Figure 6. Chondrite-normalized REE and primitive mantle-normalized multi-element diagrams of ultramafic flows (A, B), cumulates (C, D), Type I (E, F), II (G, H) and III (I, J) basalts (Normalizing value are from Sun and McDonough, 1989).

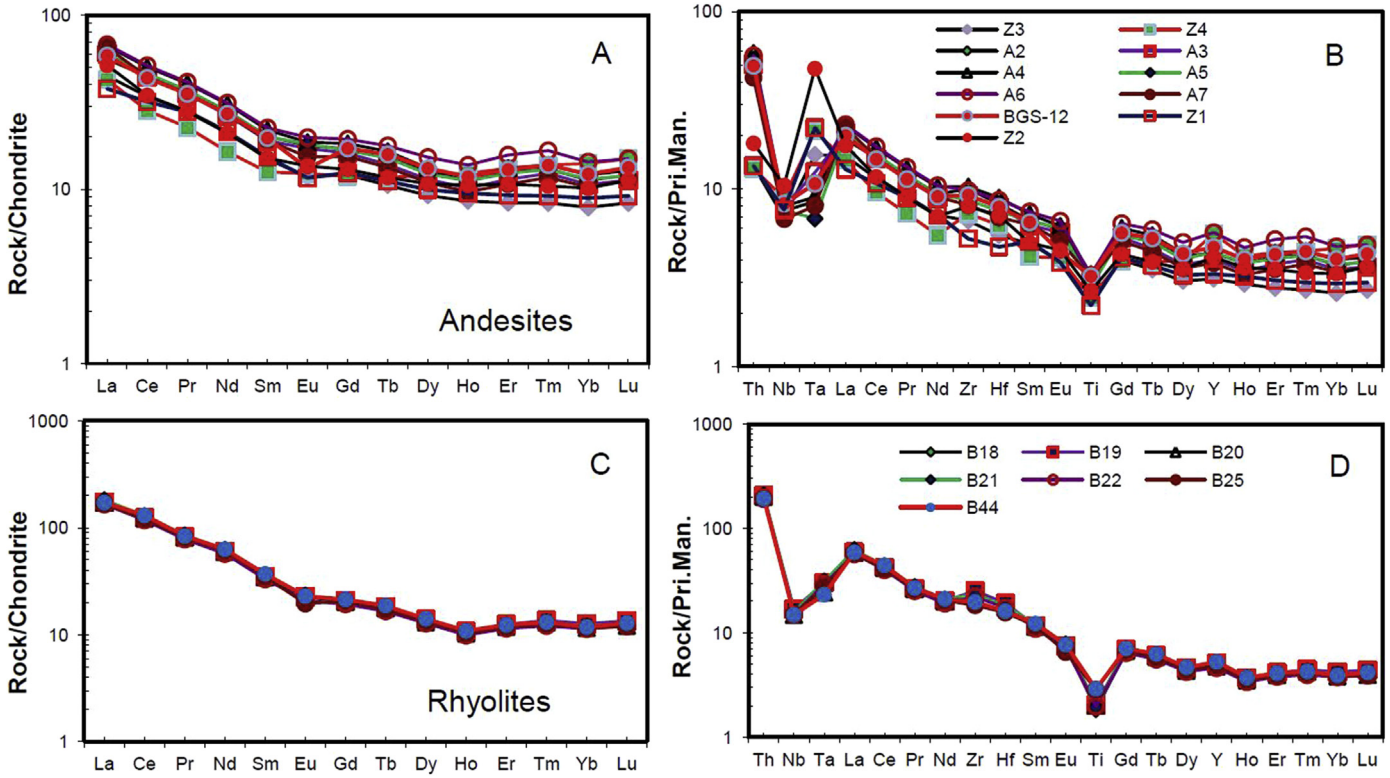

Figure 7. Chondrite-normalized REE and primitive mantle-normalized multi-element diagrams of andesite (A, B) and Dacites (C, D) Of Bundelkhand greenstone belt.

With the exception of one sample, all the other samples have Ce/Ce* within the range of 0.9 to 1.1 indicating limited LREE mobility. However, large scale negative Eu anomaly observed in komatiites reflects mobilization of Eu by high temperature hydrothermal fluids. Similar Eu anomalies observed in ultramafic rocks from other cratons of the world are generally attributed to secondary alteration processes (Sun and Nesbitt, 1978; Ludden et al., 1982; Arndt, 1994). Except two samples, all the extrusive and intrusive ultramafic rocks have <3.6 wt.% loss on ignition (LOI). Except four samples in basalts and andesites, rest of the samples are displaying <2 wt.% LOI. All the analysed samples of rhyolites have <1.5 wt.% LOI. These LOI data of the analysed samples indicate least altered nature of majority of the samples which are displaying smooth and coherent REE patterns (Manikyamba et al., 2014a). However, moderate alteration cannot be ruled out in few ultramafic and mafic rocks of the present study.

The Nb/Th ratio of primitive mantle is 8 whereas that of the Archean upper crustal value proxy by tonalites is 0.76, and hence, Nb/Th value of 8 is used as an indicator for crustally uncontaminated flows (Sun and McDonough, 1989; Rudnick and Gao, 2003; Condie, 2005). The Nb/Th ratios of majority of the analysed ultramafic rocks are greater than 8. Similar features are observed in the uncontaminated Neoarchean komatiites of the Abitibi terrane, where the ultramafics and associated tholeiitic basalts are interpreted as fragments of an oceanic plateau derived from a mantle plume erupting in an intra-oceanic setting (Xie et al., 1993). Manikyamba et al. (2008) accounted for the spectrum of Nb/Th from 8.1 to 21.2 and 3.2 to 7.2 observed in komatiites and associated tholeiitic basalts respectively in the Neoarchean Sandur greenstone terrane attest to a mantle plume erupted proximal to a rifted craton margin, wherein the values >8 represent eruption of komatiites in an oceanic domain while that of <8 were inherited from eruption through rifted continental crust.

Komatiitic basalts of the present study plot in the fields of 1, 2 and 7 in Nb/Th vs. $(La/Sm)_N$ diagram (Fig. 8a) of Said et al. (2012) implying that they are crustally uncontaminated. Apart from crustal contamination, Nb/Th ratios of the komatiites and associated tholeiitic basalts of the Kalgoorlie terrane specifically, and the larger Eastern Goldfields superterrane in general, suggest that they were generated from subduction-metasomatized lithospheric mantle during the eruption of mantle plumes at the base of the lithosphere than crustal contamination (Said et al., 2012). The variation in the Nb/Th ratios <8 of the komatiitic basalt of the present study reflect on interaction of a mantle plume with metasomatized continental mantle lithosphere. Some of the extrusive ultramafic rocks of the present study exhibit negative Nb-Ta anomalies suggesting assimilation of subduction-processed lithospheric mantle material by plume-derived magma (cf. Song et al., 2008), which is also manifested in the La/Sm versus La/Ta relationship (Fig. 8b), where the komatiitic basalts plot on the crustal contamination trend implying its role during the ascent of melts.

6.2. Mantle plume processes

Mantle plumes rise to impinge on either continental or oceanic lithospheric plates resulting in the eruption of great volumes of mafic-ultramafic melts. These eruptions form vast fields of lava flows and associated igneous complexes or oceanic islands. When the mantle plume impinges on sub-continental lithosphere, rifting may occur with subsequent eruption of continental flood basalts such as Karu, Siberian Traps and Deccan traps. Plumes when they impinge onto the mid oceanic ridge (MOR) forms large islands such as Iceland. When plumes interact with passive continental margins, thick piles of mafic rocks will be generated (ex. North Atlantic Volcanic margin) which have close links with south east coast of Greenland with Iceland. Plumes may impinge on active

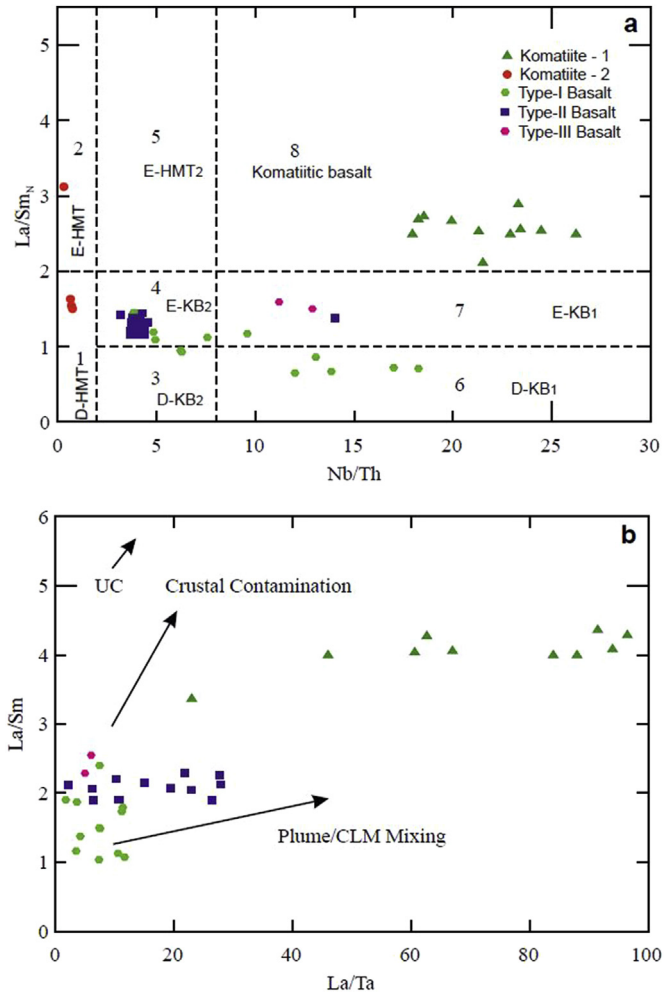

Figure 8. (a) $(La/Sm)_N$ versus Nb/Th diagram after Said et al. (2012); (b) La/Sm vs La/Ta illustrating the different trends (arrows) for contamination of plume liquids by continental lithospheric mantle (CLM).

continental margins or island arcs resulting in the generation of back-arc basins. Such lava flows associated with large igneous provinces having long lived plume activity generate from core-mantle boundary caused by the heat of the outer core (Pirajno, 2000). In the head and tail structure of the plume, the head consists of the entrained asthenospheric material whereas the tail will be hotter and generates high Mg melts of picrites and komatiites (Campbell and Griffiths, 1992; Hill et al., 1992). Therefore, the presence of high Mg lavas in the greenstone belts indicate the features of plume magmatism. A compilation of least altered komatiites from the ca. 2.7 Ga Abitibi greenstone terrane, Sproule et al. (2002) identified three types of komatiites: Ti-depleted, Al-depleted-Ti-enriched and Al-undepleted. Al-undepleted komatiites are derived from shallower or high-degree partial melting of a garnet peridotite source leaving a garnet-free residue; while Al-depleted komatiites are derived from either dynamic melting of a refractory source leaving a refractory harzburgite residue or high-degree melting of a garnet-rich source with a garnet peridotite residue and Ti-enriched komatiites are derived from partial melting of a garnet peridotite source leaving a garnet-bearing residue (Sproule et al., 2002). Based on the above criteria, two types of komatiitic basalts have been distinguished in the present study: (1) Ti-enriched-Al-depleted komatiitic basalts with low Al_2O_3/TiO_2 ratios (8.2–8.5) and (2) Al-undepleted komatiitic basalts with near-chondritic Al_2O_3/TiO_2 (13.0–18.91) ratios which are manifested in Fig. 9a.

The CaO/Al_2O_3 and Al_2O_3/TiO_2 ratios (0.6–1.78 and 13–18.91 respectively) of Al-undepleted komatiitic basalts of the present study suggest garnet inclusion into the melt phase during partial melting of mantle. The low $(La/Yb)_N$ ratios (2.7–3.6) of the studied komatiitic basalts of Al-undepleted variety corroborate high degree (>30%) of mantle melting, while $(Gd/Yb)_N$ ratios varying between 1.20 and 1.49 with negative Zr, Hf and Ti anomalies on mantle normalized multi-element diagram suggest the derivation of parent magma by melting under anhydrous conditions at shallow mantle domain where garnet is precluded from the melt phase.

The Al-depleted variety of ultramafic cumulates are composed of amphibole, pyroxene and accessory plagioclase. These rocks occur beneath the Iron Formations in Babina-Dhaura section at Pura village (Fig. 2). This ultramafic unit shows sheet like structure with a high angle dip (60°–70°) to north. Amphibole-bearing pyroxenite shows high MgO (22–25 wt.%), Al_2O_3 (9–10 wt.%), Cr (292–846 ppm), Ni (192–463 ppm), and are enriched in the Nb content (10.4–25.6 ppm). These rocks have low CaO/Al_2O_3 (0.6–1.15), Al_2O_3/TiO_2 (8.2–8.5), $(La/Yb)_N$ ratios (4.8–5.06), and $(Gd/Yb)_N$ ratios (0.39–0.44) displaying unfractionated REE patterns and exhibit negative Nb and Ta anomalies with respect to Th and positive Zr, Hf and Ti anomalies. These features reflect garnet

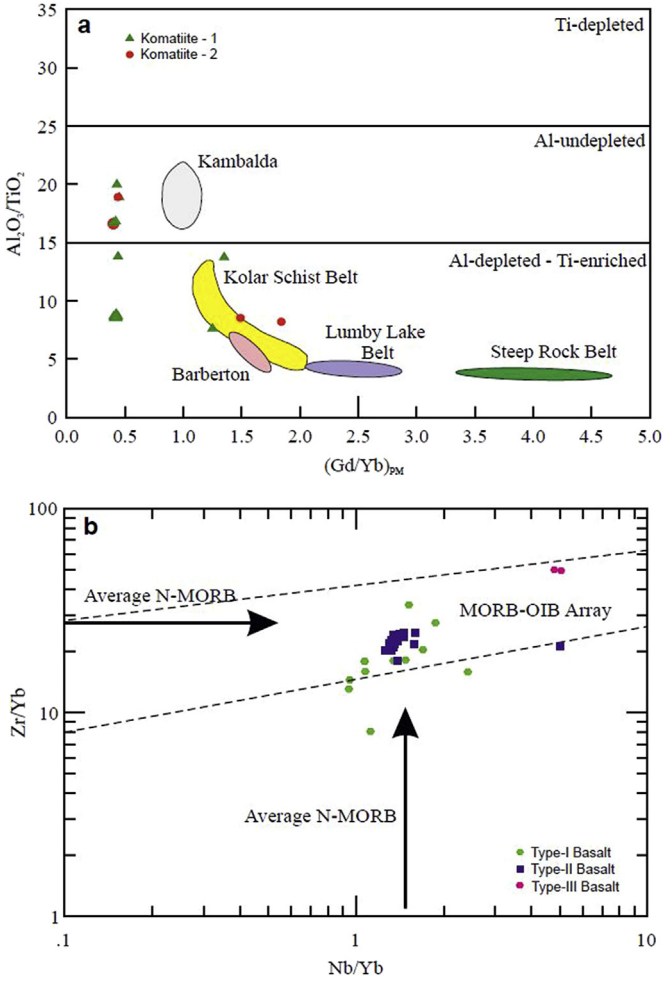

Figure 9. (a) $(Gd/Yb)_N$ vs. Al_2O_3/TiO_2 binary plot of Sproule et al. (2002) indicating ultramafics as Al-depleted and Al-undepleted varieties (b) Zr/Yb vs. Nb/Yb binary plot (modified from Macdonald et al., 2000) showing MORB-OIB affinity for three types of basalts.

inclusion into the melt phase during higher degrees of partial melting of mantle (>30%). The variation in the $(Gd/Yb)_N$ ratios (<1 and >1) for cumulates and flows suggest a garnet rich and garnet free sources from the spinel-peridotite and garnet–peridotite melting regimes are responsible for the genesis of cumulates and komatiite basalt flows respectively (Rollinson, 1999; Manikyamba et al., 2013). Therefore, the amphibole bearing pyroxenite appears to be the geochemical equivalent of Al-depleted type komatiitic basalt like those of 2.7 Ga greenstone belts of Abitibi and are geochemically similar to the Munro-type komatiites which were generated by high degree (50%), shallow level partial melting of anhydrous mantle sources. The derivation of parent magma by high degree melting of mantle at shallow depth accounted for elimination of garnet from residue. Thus, we infer that these rocks may be a part of Archean thrusted oceanic wedge component that was involved in the collision and a representative of obducted oceanic unit.

6.3. Island arc processes

6.3.1. Basalts

Fractionated LREE with HFSE/REE anomalies such as Nb, Ta, P and Ti, a characteristic feature of intraoceanic arc magmas which are resultant of slab dehydration-wedge melting processes wherein HFSE are retained in the slab whereas large ion lithophile (LILE), Th, U and LREE are contributed from slab derived fluids to the wedge (Perfit et al., 1980; Tatsumi et al., 1986; Hawkesworth et al., 1993; Pearce and Peate, 1995; Keleman et al., 2004; Pearce, 2008). Consequently, HFSE contents and HFSE/HFSE (Nb/Zr, Nb/Ta) ratios have been used to address the melt enrichment-depletion characteristics of the mantle wedge (McCulloch and Gamble, 1991; Pearce and Parkinson, 1993; Woodhead et al., 1993; Pearce et al., 2000; Pearce, 2008). Type-I basalts of the present study show flat to slightly enriched LREE patterns and lower magnitude of negative anomalies at Nb, Zr, Hf and Ti (Fig. 6H), whereas Type-II basalts exhibit pronounced negative anomalies at Nb and Ti with insignificant negative Zr and Hf anomalies. Both Type-I and Type-II basalts display relative depletion of HFSE with respect to LILE and LREE manifested in terms of high LILE/HFSE, LREE/HFSE ratios and negative Nb, Ta, Zr, Hf and Ti anomalies which are diagnostic features of subduction zone magmatism in intra-oceanic arc environments (Pearce, 2008; Manikyamba and Kerrich, 2012). Intraoceanic subduction zone characteristics such as depletion of Nb, Ta, Zr, Hf and Ti may also arise in the active continental margin lavas. According to Pearce (1983), the magnitude of enrichment in Sr, K, Rb, Ba and Th will be relatively higher in case of active continental margin tholeiites when compared to the rocks of oceanic island arc. Besides, Ce, P and Sm also show variable degrees of enrichment and the elements such as Ta, Nb, Zr, Hf, Ti, Y and Yb form a flat trend in MORB normalized patterns in the magmas generated at active continental margin. The geochemical variation in the active continental margin lavas are dependent on variable contribution of (1) subduction zone components, (2) trace element enriched sub-continental mantle, (3) partial melting, (4) fractional crystallization and (5) crustal contamination. Zr/Y ratios are used as proxy to discriminate the oceanic and continental island arc magmas (Pearce and Norry, 1979). Zr/Y vs. Zr plot clearly identify the oceanic and continental magmatic processes in these rocks (Fig. 11; Pearce, 1983). Higher abundances of Rb (0.7–44 ppm), Sr (34–655 ppm) and Zr (8–131 ppm) in Type-II basalts compared with Type-I basalts (Rb: 1–8 ppm; Sr: 68–150; Zr: 43–70 ppm) reflect contribution from subducted sediments. Mantle normalized trace element patterns of the basalts (Fig. 6) exhibit distinct peaks at U, Th and La relative to neighbouring REE. Though the magnitude of negative Nb, Ti and Hf anomalies vary from Type-I to II basalts,

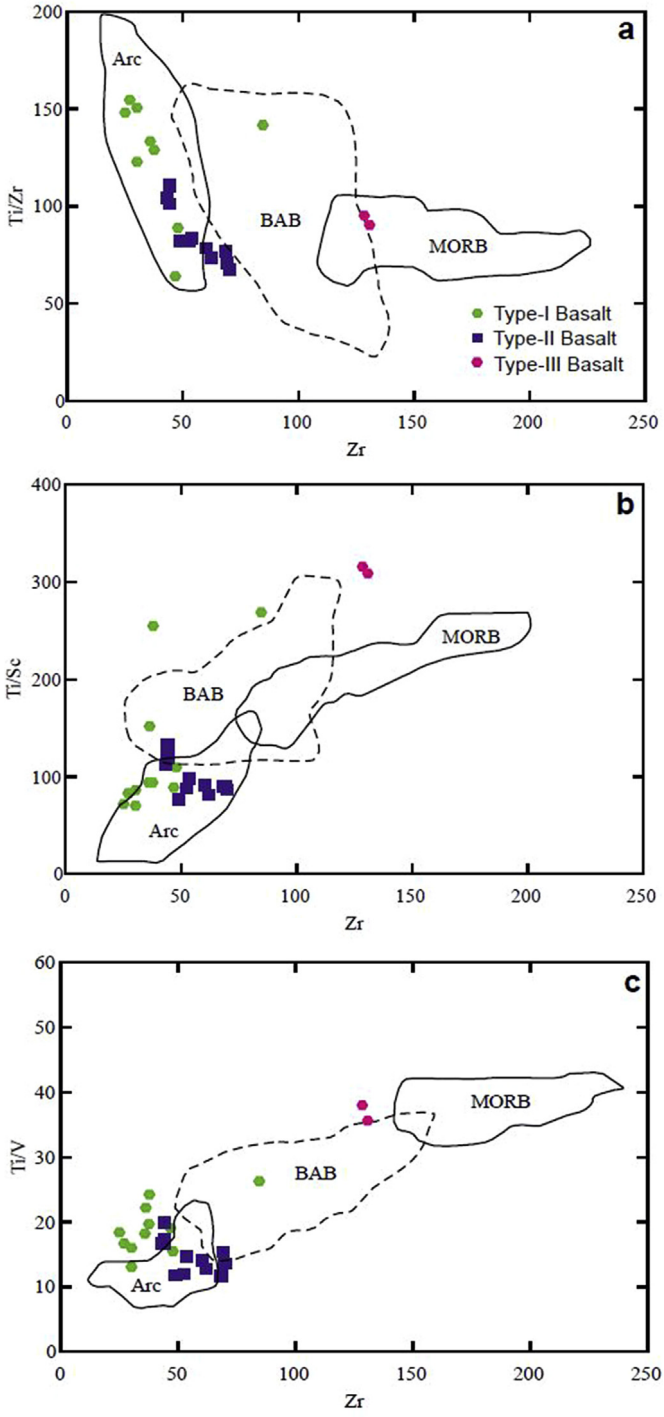

Figure 10. Tectonic discrimination diagrams of (a) Ti/Zr vs. Zr, (b) Ti/Sc vs. Zr, and (c) Ti/V vs. Zr, after Gribble et al. (1996) showing arc-back arc affinities type I, II and III basalts, andesites and dacites.

the original arc signatures are preserved in both the types. Zr/Hf and Zr/Sm ratios of Type-I basalts (33–40 and 18–26) and Type-II basalts (6–45 and 8–33) compared with primitive mantle values of 36 and 25 respectively reflect derivation of their parent magma from a depleted to enriched mantle source. The Nb depletion relative to Th is manifested in terms of Nb/Th (3–14 for Type-I and 4–18 for Type-II basalts) suggesting that source enrichment by hydrous metasomatism of the mantle wedge and varying degrees of influx of metasomatic fluids (Munker et al., 2004; Manikyamba

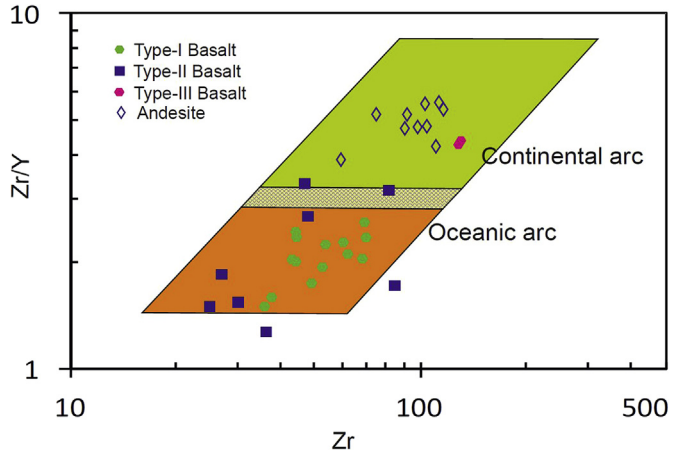

Figure 11. Zr/Y vs. Zr plot (after Pearce, 1983) reflecting on the intraoceanic to continental island arc tectonic setting for the generation of the basalts-andesites-rhyolites.

et al., 2009). The Zr/Nb ratios of Type-I (4–18) and II basalts (7–22) are consistent with the primitive arcs suggesting variable enrichment of a depleted mantle wedge in an arc environment in contrast with that of average NMORB (Zr/Nb: 11–39; Sun and McDonough, 1989; Pearce and Peate, 1995). This interpretation in also displayed in Fig. 9 where most of the data plot within the MORB-OIB array and an enriched mantle source is interpreted for their generation. It is, therefore, inferred that the hydrous metasomatism of depleted mantle wedge by slab-dehydrated fluids and minor slab-derived subducted sediment input are the sources for the enrichment of LILE and LREE of the studied basalts. The higher TiO_2 contents, lower $\sum$REE with slightly enriched LREE and absence of Eu anomalies of type III basalts compared to Type I and II varieties reflecting on the back arc nature of these basalts (Fig. 6). Thus, these three types of basalts though spatially present at different stratigraphic sequences are characterized by arc-back arc association in the Bundelkhand greenstone belt complex.

6.3.2. Andesites and Mg-andesites

Andesitic flows display composite geochemical characteristics of adakites and normal arc andesites. Adakites are generally interpreted as slab melts that hybridized with the mantle wedge in transit from the slab to the oceanic arc, acquiring enhanced Mg, Cr and Ni (Drummond et al., 1996; Martin et al., 2005). The andesites of the present study possess higher Na, Cr, Ni and Yb contents, Nb/Ta ratios and possess elevated K contents relative to normal arc andesites of the basalt–andesite–dacite–rhyolite (BADR) association (Ewart, 1979; Richards et al., 2006). In terms of SiO_2 and MgO, four of the andesitic samples qualify as magnesian andesites, also known as high-magnesian andesites (HMA). HMA are primitive, intermediate to calc-alkaline volcanic rocks having Mg# >50 with enhanced Co, Cr and Ni contents relative to normal andesites. Though, all the samples possess higher Cr contents, their Mg# and Ni contents are variable between HMA and normal andesites. They are characterized by enriched and fractionated REE ($(La/Sm)_N$ = 2.46–3.42, $(La/Yb)_N$ = 3.14–6.55, $(Gd/Yb)_N$ = 0.82–1.50; Fig. 7) and negative anomalies at Nb, Ta (except four samples) and Ti (Fig. 7A and C), a characteristic feature of volcanic arc magmas at convergent margin (Perfit et al., 1980; Hawkesworth et al., 1993; Pearce and Peate, 1995). The studied samples plot close to the spinel-garnet Iherzolite (50:50) line, in between garnet-Iherzolite and spinel-garnet Iherzolite field, with 1%–10% partial melting. In addition, the higher Nb contents (5–7 ppm) and Zr/Nb ratios (11–21) higher than those of NMORB (2.3 ppm and 11–39; Sun and McDonough, 1989), suggesting that their mantle source was heterogeneous and enriched relative to NMORB.

6.3.3. Rhyolite–rhyodacite

Hollings et al. (1999) identified two types of felsic volcanic rocks (Type 1 and Type 2) associated with komatiite–tholeiite sequence from the greenstone belts of northern Superior Province. Type 1 rhyolites have relatively aluminous compositions with strongly fractionated REE patterns which are comparable with Cenozoic adakites and Archean high-Al TTG suites. Both Type 1 and Type 2 rhyolites show LREE enriched patterns and negative Nb and Ti anomalies, but Type 1 rhyolites has strongly fractionated HREE patterns compared to flat HREE with elevated Ni and Cr contents of Type 2 rhyolites. Type 1 rhyolites are comparable to southern Superior Province felsic volcanic rocks associated with oceanic arc sequences and inferred to be the products of oceanic slab melting. The geochemical signatures of Type 2 rhyolites are explained to be the products of mixing of Type 1 rhyolites with tholeiitic magmas, or a contribution from mantle wedge sources located above the garnet stability field. Hollings and Kerrich (2000) reported Type 3 rhyolites from the arc basalt-Nb-enriched basalt-adakite association of 2.7 Ga Birch-Uchi greenstone belt. Type 3 rhyolites, characterized by moderate LREE fractionation, flat HREE, pronounced negative Eu and Ti anomalies, are interpreted to be the products of intra-crustal fractional crystallization of basaltic liquids. The geochemical characteristics of studied rhyolitic samples, marked by aluminous composition with low and fractionated HREE patterns and minor negative Eu anomalies, are in conformity with Type-I rhyolites. Th, Yb and Zr variations (Fig. 7B) show low order negative anomalies in the studied rhyolites. On the basis of their geochemical signatures, rhyolites are further classified as FI (calc-alkaline, low HFSE, moderate to high Zr/Y, $(La/Yb)_N$ = 5.8–34, strong subduction signatures), FII (calc-alkaline to transitional, intermediate HFSE, moderate Zr/Y, La/Yb_N = 1.7–8.8; prominent subduction signatures, FIIIa (tholeiitic, moderate HFSE, low Zr/Y, $(La/Yb)_N$ = 1.5–3.5, weak subduction signatures) and FIIIb (tholeiitic, high HFSE and HREE, low Zr/Y, $(La/Yb)_N$ = 1.1–4.9, no subduction signatures) types (Lesher et al., 1986). The geochemical characteristics of the analysed rhyolites are marked by high silica, calc-alkaline nature, Th and La enrichment, variably fractionated LREE/HREE patterns, low HFSE and moderate to high Zr/Y and $(La/Yb)_N$ (9–12 and 20.2–17.1, respectively) indicate their similarity with F1 type rhyolites from Archean greenstone belts of different cratons (Lesher et al., 1986). The Archean FI rhyolites are interpreted to be generated by partial melting of thick basaltic crust metamorphosed to amphibolite/eclogite at ~40 km. The rhyolites of F1 type are suggested to have formed at depths of >30 km with a garnet bearing mantle residue whereas FII rhyolites from depths ranging from 10 to 30 km with amphibole-plagioclase residue and FIII type corresponds at <15 km in depth with plagioclase dominant garnet-amphibole free residue (Hart et al., 2004). The rhyolites of the present study are, thus, interpreted to be the products of partial melting of thick basaltic crust metamorphosed to amphibolite/eclogite facies at depths ranging from as high as 30 to 10 km with garnet and amphibole-plagioclase-bearing mantle residue. Few basaltic flows (Type-III) of present studies are associated with these rhyolites exhibit moderate MgO (7–8 wt.%); high TiO_2(~2 wt.%), Na_2O (~2 wt.%), Zr (~128 ppm), Nb (~13 ppm) and Zr/Y (8–13); low LREE/HFSE ratio $(La/Yb)_N$ = 3.2–3.4); HFSE/HFSE ratio (Zr/Hf = 37–39). The high zirconium and niobium contents of these basalts also testify their derivation from a similar magma source as rhyolites. The REE and multi element distribution patterns (Figs. 6 and 7) of basalts indicate the metasomatic signature at the source. Thus,

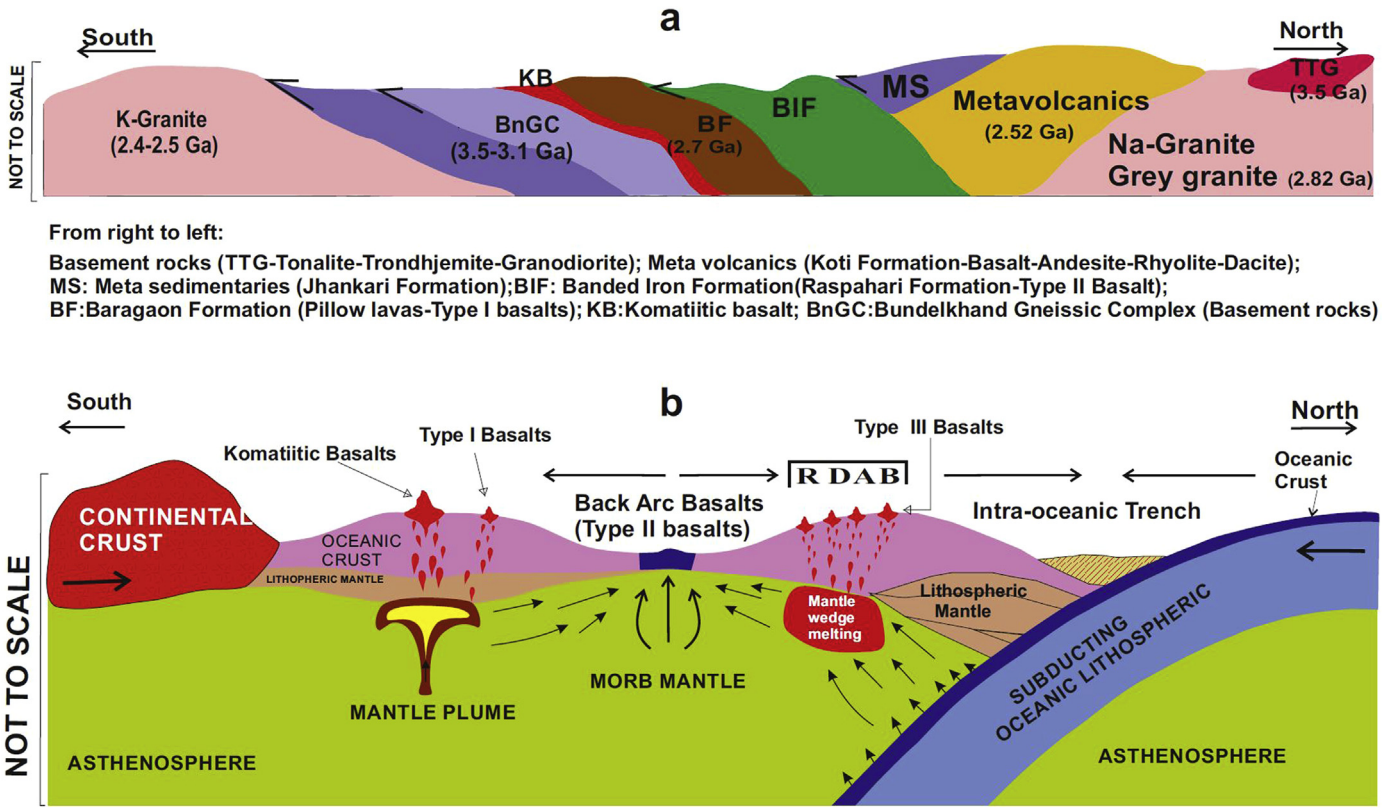

Figure 12. (a) Schematic model showing genesis of Type I, II basalts along the andesite–rhyolite-dacite sequence in an intra-oceanic island arc setting, Type III basalts are erupted in a back-arc-basin setting. The komatiitic basalts were erupted through mantle plume in an ocean crust (Vertical and horizontal- Not to Scale) and (b) Schematic cross section representing presently exposed sequence of Bundelkhand Greenstone Belt at Mauranipur area (not to scale).

collectively these characteristics indicate that the associated basaltic flows are less fractionated and bear a similar magma source of studied rhyolites.

6.4. Geodynamic implications

Typical island arc lavas are enriched in LILE and LREE, but depleted in HFSE, particularly in Nb, Ta, and Ti on normalized trace element diagrams (Saunders et al., 1991; Hawkesworth et al., 1993; Hawkins, 2003; Pearce, 2003; Murphy, 2007). On Zr/Yb vs. Nb/Yb diagram of Macdonald et al. (2000) (Fig. 9b) komatiites plot near OIB on the MORB-OIB array, whereas basalts scatter in between NMORB and EMORB and plot close to the upper boundary of the MORB-OIB array. MORB-OIB array stems from shallow melting of depleted upper mantle asthenosphere for MORB, but deeper melting of a relatively enriched source for OIB, likely from a plume originating in the deeper mantle (Pearce, 2008). The CaO/Al_2O_3 ratio more than unity with very high MgO contents (>20 wt.%), $(Gd/Yb)_N$ in the range of 1.18–1.80 and positive Nb anomalies of the studied komatiitic basalts are indicative of mantle plume source for their origin (Xie et al., 1993; Kerrich and Xie, 2002; Pearce, 2008). Type-I, II and III basalts of the present study occupy the fields of arc and back arc on Ti/Zr, Ti/Sc and Ti/V vs. Zr plots (Fig. 10; Gribble et al., 1996), strongly suggests an intraoceanic tectonic setting for the generation of these rock types. However, type-III basalts are characterized by LREE enrichment relative to HREE and a feeble negative Eu anomaly (Fig. 6J). Enrichment of HFSE over HREE, with a concave downward pattern in primitive mantle normalized multielement plot (Fig. 6I), suggests that the type-III basalts were generated by melting of a relatively enriched source at greater depth. Further, they plot closer to OIB on the MORB-OIB array in the Zr/Yb vs. Nb/Yb diagram of Macdonald et al. (2000) (Fig. 9b) reflecting oceanic island setting for their generation.

The enrichment of LILE (e.g. Cs, Rb Ba, Th, K and U) and depletion of HFSE (e.g. Zr, Hf, Nb, Ta, Y, Ti) relative to typical primitive mantle values, negative Nb-Ta, Zr-Hf anomalies, and positive Th anomalies (Fig. 7C and D) for the studied andesites and rhyolites are in compliance with the geochemical characteristics of magmas generated in subduction-related tectonic settings. Ta, Yb, Th and Hf are used to discriminate felsic-intermediate compositions (54–77 wt.% SiO_2) that are erupted from oceanic arcs, active continental margins, and within-plate volcanic zones (Schandl and Gortol, 2002; Wang et al., 2008). The Zr/Y vs. Zr variations in the studied samples indicate active continental margin setting (Fig. 11). The Th enrichment in the studied samples may reflect the influence of the subduction derived fluids.

The recycling of Archean crust into the subduction zones generating more diversified mafic and felsic volcanic rocks (BADR) of tholeiitic to calc-alkaline affinity which has been witnessed worldwide in many Archean greenstone belts such as south western Greenland, Pilbara craton; Belingwe greenstone belt, Zimbabwe; Dharwar and Singhbhum Cratons of India (Nisbet et al., 1987; Eriksson et al., 1994; Smithies et al., 2005; Manikyamba and Kerrich, 2012; Polat, 2013; Manikyamba et al., 2014b; Rajanikanta Singh et al., 2017). Presence of different types of basalts and BADR type of differentiation at Baragaon and Babina-Koti areas in the east and west of the greenstone belt respectively demarcate a distinct genetic origin and involvement of mantle processes in the genesis of ultramafic-mafic-felsic magmatism (Fig. 12a and b). Further, their close temporal association observed in various locations Baragaon, Babina, Koti and Dhaura may also reflect on fractional crystallization in a sub-arc environment. Such calc-

alkaline series have been reported from Salina, Aeolian arc, Italy (Gertisser and Keller, 2000). The Nb-enriched ultramafic flows of Baragaon (11.2–25.6 ppm) may represent an OIB like remnant of ocean crust which was obducted at the late stages of convergence. Ce (27–56 ppm) in ultramafic cumulates, (1.89–3.5 ppm) in flows, (2.81–29.89 ppm) of basalts, (17.0–30.9 ppm) of Mg-andesites and very low Yb (0.1–4.0 ppm) contents of all the above attests to intraoceanic Island arcs such as Tonga-Kermadec and South Sandwich that have very low Ce contents, whereas Marianas, Aleutians, New Britain and Andes SVZ are indicated by moderate Ce contents up to 40 ppm (Hawkesworth et al., 1993). Komatiite basalts occur at the bottom-most horizon in the stratigraphy of the greenstone sequence conformably in contact with crystalline basement which is a characteristic lithological unit of Bundelkhand greenstone belt (Fig. 12b). Such stratigraphy clearly indicates the obduction of remnant oceanic crust during complete convergence at a much faster rate (e.g. Isua greenstone belt, Komiya et al., 1999). The plume generated ultramafic rocks are associated with island arc volcano-sedimentary sequences of Baragaon (komatiite–basalt–dacite–rhyolite and BIF). These litho units are continued into Babina (andesites–rhyolites; cherts and BIFs), which are in turn continued into Umri where the ultramafic-mafic rocks directly resting on BIFs (at Pura village). The rocks of this Formation again appear towards north at Sugeswarashram (shown as Temple in Fig. 1C) with ultramafic cumulates overlain by metasediments (fuchsite quartzite, greywackes). These geological relationships and geochemical characteristics reflect on the plume–arc accretion in this part of Bundelkhand craton.

Similar type of ultramafics, pillow basalts, basalt–andesite–dacite–rhyolite and BIF associations trending in N–S to NNE–SSE greenstone belts from EDC (Sandur, Hutti, Penakacherla and Gadwal, Kadiri, Veligallu) have been reported from the southern part of Indian shield at nearly same geological time (Polat et al., 2011; Kerrich and Manikyamba, 2012; Manikyamba and Kerrich, 2012; Jayananda et al., 2013) where convergent margin tectonic setting with plume interaction have been proposed.

Studies in the southern Indian shield have revealed evidence for extensive crustal growth through arc magmatism during the Meso- and Neoarchean times (Santosh et al., 2015). The 3.3–2.5 Ga volcano-sedimentary greenstone sequences of Dharwar Craton are characterized by either komatiite–tholeiite association that has been interpreted to be the product of plume magmatism and plume–lithosphere interaction or tholeiitic to calc–alkaline basalt–andesite–dacite–rhyolite (BADR) volcanic sequences along with boninites, Nb-enriched basalts, adakites, Mg-andesites, shoshonites, leucitites and arc basalts considered to be the products of subduction–accretion processes (Ananta Iyer et al., 1980; Rajamani et al., 1985; Balakrishnan et al., 1990; Giritharan and Rajamani, 1998; Manikyamba et al., 2012, 2014a,b, 2015a,b).

The geochemical plots of rocks of E–W trending greenstone belt of Bundelkhand discriminate intraoceanic island arc to back arc to active continental margin setting and their accretion with the plume generated mafic-ultramafic magmas (Fig. 12) in the north of Son Narmada lineament for the Bundelkhand greenstone belt.

7. Conclusions

On the basis of field, petrographic and geochemical data of the major rock formations from the greenstone belt in the Bundelkhand craton, we arrive at the following conclusions.

(1) Four lithostratigraphic Formations and stratigraphic columns are identified in the Bundelkhand greenstone belt. These are the Baragaon (predominantly high Mg pillow basalts and Mg andesite), Raspahari (dominated by BIF, basaltic, cherts and other chemogenic sediments), Umari/Jhankari (with arkosic, argillaceous and arenaceous types of supracrustal sediments) and Koti Formations (dominated by rhyolites, andesite, rhyodacite, granite breccias, tuffs with rare basic flows) and are characterized by distinct mafic and felsic flows are identified.
(2) The ultramafic units of komatiitic basalts at Baragaon and amphibole bearing pyroxenite cumulate at Pura village from Baragaon Formation are stratigraphically and compositionally distinct and represent probable remnants of oceanic crust.
(3) Type I, II and III basalts have been identified which are associated with various lithologies and exhibit overlapping to variable geochemical characteristics reflecting on arc-back-arc association in the Bundelkhand greenstone terrain.
(4) The associated intermediate to felsic volcanic rocks were derived from partial melting of thick basalt crust metamorphosed to amphibolite to eclogite facies at a depth of around 30–40 km.
(5) The eastern part, where basalts of Baragaon Formation are associated with chemogenic sediments (BIF) of Raspahari Formation, has least contaminated mafic and ultramafic flows followed by andesite-Mg andesite, whereas the central part of greenstone belt at Dhaura (Koti Formation), Raspahari Formations are dominated by felsic volcanics, basalts, tuffs and breccia of rhyodacites. The rocks in the extreme western part Umari-Jhankari of the greenstone belt, developed around Mohar are dominated by supracrustal felsic volcanics and tuffs, similar to those Koti Formation are characterized by high abundances of crustal components.
(6) Our study suggests plume-arc accretionary tectonics for the greenstone belt sequences at Mauranipur, Babina-Dhaura and Umari-Jhankari areas of Bundelkhand Craton.

Acknowledgements

The authors are grateful to Dr. V.M. Tiwari, Director, CSIR-NGRI for his kind encouragement and support to publish this work. Drs. C.M and K.S.V.S acknowledges the funds from Council of Scientific and Industrial Research (CSIR) to National Geophysical Research Institute under MLP 6201-28 (CM). SPS is thankful to Ministry of Earth Sciences, Government of India for the financial support (MoES/P.O.(Geosci)/4/2013). The authors thank the two anonymous reviewers for their critical and constructive comments. We thank Dr. Sohini Ganguly for efficient editorial handling. Dr. M. Satyanarayanan, S.S. Sawant, and A. Kehsav Krishna are acknowledged for help in the analytical work.

Appendix A. Supplementary data

Supplementary data related to this article can be found at https://doi.org/10.1016/j.gsf.2017.08.008.

References

Ananta Iyer, G.V., Vasudev, V.N., Jayaram, S., 1980. Rare earth element geochemistry of metabasalts from Kolar and Hutti gold-bearing volcanic belts, Karnataka Craton, India. Journal of the Geological Society of India 21, 603–608.
Arndt, N., Lesher, C.M., 2004. Komatiite. Encyclopaedia of Geology. Elsevier, pp. 260–268.
Arndt, N.T., 1994. Archean komatiites. In: Condie, K.C. (Ed.), Archean Crustal Evolution, Developments in Precambrian Geology, vol. 11. Elsevier, Amsterdam, pp. 11–44.
Arndt, N.T., Nisbet, E.G., 1982. What is a komatiite? In: Arndt, N.T., Nisbet, E.G. (Eds.), Komatiites. George Allen and Unwin publications, London, pp. 19–28.

Balakrishnan, S., Hanson, G.N., Rajamani, V., 1990. Pb and Nd isotope constraints on the origin of high Mg and tholeiitic amphibolites, Kolar schist belt, south India. Contributions to Mineralogy and Petrology 107, 279–292.
Baitsch-Ghirardello, B., Gerya, T.V., Burg, J.P., 2014. Geodynamic regimes of intra-oceanic subduction: implications for arc extension vs. shortening processes. Gondwana Research 25, 546–560.
Basu, A.K., 1986. Geology of Parts of the Bundelkhand Granite Massif, Central India. In: Records of Geological Survey of India, Special Publication, vol. 117, pp. 61–124.
Benn, K., Mareschal, J., Condie, K.C., 2006. Introduction: Archean Geodynamics and Environments. In: Geophysical Monograph Series, vol. 164. American Geophysical Union, Washington D.C., pp. 1–5
Bhattacharya, A.R., Singh, S.P., 2013. Proterozoic crustal scale shearing in the Bundelkhand Massif with special reference to quartz reefs. Journal of the Geological Society of India 82, 474–484.
Braun, J.J., Pagel, M., Herbillon, A., Rosin, C., 1993. Mobilization and redistribution of REEs and thorium in a syenitic lateritic profile—a mass-balance study. Geochimica et Cosmochimica Acta 57, 4419–4434.
Campbell, I.H., Griffiths, R.W., 1992. The changing nature of mantle hotspots through time: implications for the chemical evolution of the mantle. The Journal of Geology 100, 497–523.
Condie, K.C., 2005. TTG and adakites: are they both slab melts? Lithos 80, 33–44.
Condie, K.C., 2000. Episodic continental growth models: after thoughts and extensions. Tectonophysics 322, 153–162.
De Joux, A., Thordarson, T., Fitton, J.G., Hastie, A.R., 2014. The Cosmos greenstone succession, Agnew-Wiluna greenstone belt, Yilgarn Craton, Western Australia: geochemistry of an enriched Neoarchean volcanic arc succession. Lithos 205, 148–167.
Drummond, M.S., Defant, M.J., Kepezhinskas, P.K., 1996. Petrogenesis of slab-derived trondhjemite–tonalite–dacite/adakite magmas. Transactions of the Royal Society of Edinburgh – Earth Sciences 87, 205–215.
Eriksson, K.A., Krapez, B., Fralick, P.W., 1994. Sedimentology of Archean greenstone belts: signatures of tectonic evolution. Earth-science Reviews 37, 1–88.
Ewart, A., 1979. A review of the mineralogy and chemistry of Tertiary-Recent dacitic, latitic, rhyolitic and related salic volcanic rocks. In: Barker, F. (Ed.), Trondhjemites, Dacites and Related Rocks. Elsevier, Amsterdam, pp. 13–121.
Furnes, H., Wit, M.D., Dilek, Y., 2014. Four billion years of ophiolites reveal secular trends in oceanic crust formation. Geoscience Frontiers 5, 571–603.
Gertisser, R., Keller, J., 2000. From basalt to dacite: origin and evolution of the calc-alkaline series of Salina, Aeolian Arc, Italy. Contributions to Mineralogy and Petrology 139, 607–626.
Gribble, R.F., Stem, R.J., Bloomer, S., Stuben, D., Ohearn, T., Newman, S., 1996. MORB mantle and subduction components interact to generate basalts in the southern Mariana through back-arc basin. Geochimica et Cosmochimica Acta 60, 2153–2166.
Giritharan, T.S., Rajamani, V., 1998. Geochemistry of the metavolcanics of the Hutti-Maski Schist Belt: implications to gold metallogeny in the eastern Dharwar Craton. Journal of the Geological Society of India 51, 583–594.
Hart, T.R., Gibson, H.L., Lesher, C.M., 2004. Trace element geochemistry and petrogenesis of felsic volcanic rocks associated with volcanogenic massive Cu-Zn-Pb sulfide deposits. Economic Geology 99, 1003–1013.
Hawkesworth, C.J., Gallagher, K., Hergt, J.M., McDermott, F., 1993. Mantle and slab contributions in arc magmas. Annual Reviews of Earth and Planetary Science Letters 21, 175–204.
Hawkins, J.W., 2003. Geology of supra-subduction zones—implications for the origin of ophiolites. In: Dilek, Y., Newcomb, S. (Eds.), Ophiolite Concept and the Evolution of Geological Thought, Geological Society of America Special Paper 373, pp. 227–268.
Hill, R.I., Chappell, B.W., Campbell, I.H., 1992. Late Archaean granites of the southeastern Yilgarn Block, Western Australia: age, geochemistry, and origin. Transactions of the Royal Society of Edinburgh: Earth Sciences 83, 211–226.
Hollings, P., Kerrich, R., 2000. An Archean arc basalt-Nb enriched basalt-adakite association: the 2.7 Ga confederation assemblage of the Birch–Uchi greenstone belt, superior province. Contributions to Mineralogy and Petrology 139, 208–226.
Hollings, P., Wyman, D., Kerrich, R., 1999. Komatiite-basalt-rhyolite volcanic associations in northern superior province greenstone belts: significance of plume-arc interaction in the generation of the proto continental superior province. Lithos 46, 137–161.
Irvine, T.N., Baragar, W.R.A., 1971. A guide to the chemical classification of the common igneous rocks. Canadian Journal of Earth Sciences 8, 523–548.
Isley, A.E., Abbott, D.H., 1999. Plume-related mafic volcanism and the deposition of banded iron formation. Journal of Geophysical Research 104, 461–477.
Jayananda, M., Peucat, J.J., Chardon, D., Krishna Rao, B., Fanning, C.M., Corfu, F., 2013. Neoarchean greenstone volcanism and continental growth, Dharwar craton, southern India: constraints from SIMS U-Pb zircon geochronology and Nd isotopes. Precambrian Research 227, 55–76.
Joshi, K.B., Bhattacharjee, J., Rai, G., Halla, J., Kurhilla, M., Heilimo, E., Ahmad, T., Whitehouse, M., 2013. High-K Granitoids from Bundelkhand Craton: Manifestation Near Archean – Proterozoic Transition. International Association for Gondwana Research Conference Series No. 16, 3rd International Conference Precambrian Continental Growth and Tectonism, Jhansi, 67–68.
Kaur, P., Zeh, A., Chaudhari, N., 2014. Characteristic of U–Pb–Hf isotope record of the 3.55 Ga felsic crust from the Bundelkhand Craton, Northern India. Precambrian Research 255, 236–244.
Kaur, P., Zeh, A., Chaudhri, N., Eliyas, N., 2016. Unravelling the record of Archaean crustal evolution of the Bundelkhand Craton, northern India using U–Pb zircon–monazite ages, Lu–Hf isotope systematics, and whole-rock geochemistry of granitoids. Precambrian Research 281, 384–413.
Keleman, P.B., Hanghoj, K., Greene, A.R., 2004. One view of the geochemistry of subduction-related magmatic arcs with an emphasis on primitive andesite and lower crust. In: Rudnick, R.L., Holland, H.D., Turekian, K.K. (Eds.), Treatise on Geochemistry, vol. 3, pp. 593–659.
Kerrich, R., Xie, Q., 2002. Compositional recycling structure of an Archean superplume: Nb-Th-U-LREE systematics of Archean komatiites and basalts revisited. Contributions to Mineralogy and Petrology 142, 476–484.
Kerrich, R., Polat, A., 2006. Archean greenstone-tonalite duality: thermochemical mantle convection models or plate tectonics in the early Earth global dynamics? Tectonophysics 415, 141–165.
Kerrich, R., Manikyamba, C., 2012. Contemporaneous eruption of Nb-enriched basalts – K-adakites – Na-adakites from the 2.7 Ga Penakacherla terrane: implications for subduction zone processes and crustal growth in the eastern Dharwar craton, India. Canadian Journal of Earth Sciences 49, 615–636.
Komiya, T., Maruyama, S., Masuda, T., Nohda, S., Hayashi, M., Okamoto, K., 1999. Plate tectonics at 3.8-3.7 Ga: field evidence from the Isua accretionary complex, Southern West Greenland. The Journal of Geology 107, 515–554.
Kumar, S., Raju, K., Pathak, M., Pandey, A., 2010. Magnetic susceptibility mapping of felsic magmatic lithounits in the central part of Bundelkhand Massif, central India. Journal of the Geological Society of India 75, 539–548.
Kumar, S., Yi, K., Raju, K., Pathak, M., Kim, N., Lee, T.H., 2011. SHRIMP U–Pb geochronology of felsic magmatic lithounits in the central part of Bundelkhand Craton, Central India. In: Molina, J.F.S., Scarrow, J.H., Bea, F., Montero, P. (Eds.), 7th Hutton Symposium on Granites and Related Rocks Avila, Spain, p. 83.
Krishna, A.K., Murthy, N.N., Govil, P.K., 2007. Multi-element analysis of soils by wavelength-dispersive x-ray fluorescence spectrometry. Atomic Spectroscopy 28, 202–214.
Lahaye, Y., Arndt, N.T., 1996. Alteration of a komatiite flow from Alexo, Ontario. Journal of Petrology 37, 1261–1284.
Lesher, C.M., Goodwin, A.M., Campbell, I.H., Gorton, M.P., 1986. Trace element geochemistry of ore associated and barren felsic metavolcanic rocks in the Superior Province, Canada. Canadian Journal of Earth Sciences 23, 222–237.
Lesher, C.M., Stone, W.E., Arndt, N.T., 1997. Nd Isotope Geochemistry of Komatiites in the Abitibi-Pontiac Greenstone Belt. Geological Association of Canada-Mineralogical Association of Canada Annual Meeting, Ottawa, Program with Abstracts 22, p. A88.
Lesher, C.M., Stone, W.E., 1996. Exploration geochemistry of komatiites. In: Wyman, D.A. (Ed.), Igneous Trace Element Geochemistry: Applications for Massive Sulphide Exploration, Short Course, vol. 12. Geological Association of Canada, pp. 153–204.
Ludden, J., Gelienas, L., Trudel, P., 1982. Archean metavolcanics from the Rouyn–Noranda district, Abitibi greenstone belt, Quebec: 2. Mobility of trace elements and petrogenetic constraints. Canadian Journal of Earth Sciences 19, 2276–2287.
Macdonald, R., Hawkesworth, C.J., Heath, E., 2000. The Lesser Antilles volcanic chain: a study in arc magmatism. Earth-science Reviews 49, 1–76.
Malviya, V.P., Arima, M., Pati, J.K., Kaneko, Y., 2006. Petrology and geochemistry of metamorphosed basaltic pillow lava and basaltic komatiite in the Mauranipur area: subduction related volcanism in the Archean Bundelkhand craton, Central India. Journal of Mineralogical and Petrological Sciences 101, 199–217.
Manikyamba, C., Naqvi, S.M., Ram Mohan, M., Gnaneshwar Rao, T., 2004. Remnant of an Archean subduction complex and its relationship with gold mineralisation and hydrothermal alterations – an example from Penakacherla schist belt, Dharwar Craton, India. Ore Geology Reviews 24, 199–227.
Manikyamba, C., Naqvi, S.M., Subba Rao, D.V., Rammohan, M., Khanna, Tarun C., Rao, T.G., Reddy, G.L.N., 2005. Neoarchean Boninites-implications for Archean subduction processes. Earth and Planetary Science Letters 230, 65–83.
Manikyamba, C., Khanna, T.C., 2007. Crustal growth processes as illustrated by the Neoarchean intraoceanic magmatism from Gadwal greenstone belt, eastern Dharwar craton, India. Gondwana Research 11, 476–491.
Manikyamba, C., Kerrich, R., Khanna, T.C., Krishna, A.K., Satyanarayanan, M., 2008. Geochemical systematics of komatiite–tholeiite and adakite–arc basalt associations: the role of a mantle plume and convergent margin in formation of the Sandur Super terrane, Dharwar craton, India. Lithos 106, 155–172.
Manikyamba, C., Kerrich, R., Khanna, T.C., Satyanarayanan, M., Krishna, A.K., 2009. Enriched and depleted arc basalts, with high-Mg andesites and adakites: a potential paired arc–back arc of the 2.7 Ga Hutti greenstone terrane, India. Geochimica et Cosmochimica Acta 73, 1711–1736.
Manikyamba, C., Kerrich, R., 2012. Eastern Dharwar Craton, India: continental lithosphere growth by accretion of diverse plume and arc terranes. Geoscience Frontiers 3, 225–240.
Manikyamba, C., Kerrich, R., Polat, A., Raju, K., Satyanarayanan, M., Krishna, A.K., 2012. Arc picrite–potassic adakitic–shoshonitic volcanic association of the Neoarchean Sigegudda greenstone terrane, western Dharwar craton: transition from arc wedge to lithosphere melting. Precambrian Research 212, 207–224.

Manikyamba, C., Kerrich, R., Polat, A., Saha, Abhishek, 2013. Dharwar Craton, India: evidence for compositional diversity in Archean mantle plumes. Lithos 177, 120–135.
Manikyamba, C., Saha, A., Ganguly, S., Santosh, M., Lingadevaru, M., Singh, M.R., Subba Rao, D.V., 2014a. Sediment-infill volcanic breccias from the Neoarchean Shimoga greenstone terrane, western Dharwar Craton: implications on pyroclastic volcanism and sedimentation in an active continental margin. Journal of Asian Earth Sciences 96, 269–278.
Manikyamba, C., Ganguly, Sohini, Saha, Abhishek, Santosh, M., Rajanikanta Singh, M., Subba Rao, D.V., 2014b. Continental lithospheric evolution: constraints from the geochemistry of felsic volcanic rocks in the Dharwar Craton, India. Journal of Asian Earth Sciences 95, 65–80.
Manikyamba, C., Saha, A., Santosh, M., Ganguly, S., Rajnikanta Singh, M., Subba Rao, D.V., Lingadevaru, M., 2014c. Neoarchaean felsic volcanic rocks from the Shimoga greenstone belt, Dharwar Craton, India: geochemical fingerprints of crustal growth at an active continental margin. Precambrian Research 252, 1–21.
Manikyamba, C., Ganguly, Sohini, Santosh, M., Rajanikanta Singh, M., Saha, Abhishek, 2015a. Arc-nascent back arc signature in metabasalts from the Neoarchean Jonnagiri greenstone terrane, Eastern Dharwar Craton. Geological Journal 50, 651–669.
Manikyamba, C., Jyotisankar, Ray, Ganguly, Sohini, Rajanikanta Singh, M., Santosh, M., Saha, Abhishek, Satyanarayanan, M., 2015b. Boninitic metavolcanic rocks and island arc tholeiites from the Older Metamorphic Group (OMG) of Singhbhum Craton, eastern India: geochemical evidence for Archean subduction processes. Precambrian Research 271, 138–159.
Martin, H., Smithies, R.H., Rapp, R., Moyen, J.-F., Champion, D., 2005. An overview of adakites, tonalite–trondhjemite–granodiorite (TTG) and sanukitoid: relationships and some implications for crustal evolution. Lithos 79, 1–24.
McCulloch, M.T., Gamble, A.J., 1991. Geochemical and geodynamical constraints on subduction zone magmatism. Earth and Planetary Science Letters 102, 358–374.
Mohan, M.R., Singh, S.P., Santosh, M., Siddiqui, M.A., Balaram, V., 2012. TTG suite from the Bundelkhand Craton, central India: geochemistry, petrogenesis and implications for Archean crustal evolution. Journal of Asian Earth Sciences 58, 38–50.
Mondal, M.E.A., Goswami, J.N., Deomurari, M.P., Sharma, K.K., 2002. Ion microprobe $^{207}Pb/^{206}Pb$ ages of Zircons from the Bundelkhand massif, northern India, implications for crustal evolution of the Bundelkhand-Aravalli Proto-continent. Precambrian Research 117, 85–110.
Mondal, M.E.A., Sharma, K.K., Rahman, A., Goswami, J.N., 1998. Ion microprobe $^{207}Pb/^{206}Pb$ zircon ages for the gneisses-granitoids rocks from Bundelkhand massif: evidence for the Archean components. Current Science 74, 70–75.
Munker, C., Worner, G., Yogodzinski, G., Churikova, T., 2004. Behaviour of high field strength elements in subduction zones: constraints from Kamchatka–Aleutian arc lavas. Earth and Planetary Science Letters 224, 275–293.
Murphy, J.B., 2007. Arc magmatism II: geochemical and isotopic characteristics. Geoscience Canada 34, 7–35.
Nisbet, E.G., et al., 1987. Uniquely fresh komatiites from the Belingwe greenstone belt, Zimbabwe. Geology 15, 1147–1150.
O'Hanley, D.S., 1997. Serpentinites and rodingites as records of metasomatism and fluid history. Oxford Monographs of Geology and Geophysics 35, 164–175.
Ordóñez-Calderón, J.C., Polat, A., Fryer, B.J., Gagnon, J.E., Raith, J.G., Appel, P.W.U., 2008. Evidence for HFSE and REE mobility during calc-silicate metasomatism, Mesoarchean (~3075 Ma) Ivisaartoq greenstone belt, southern West Greenland. Precambrian Research 161, 317–340.
Pandey, U.K., Bhattacharya, D., Sastry, D.V.L.N., Pandey, B.K., 2011. Geochronology (Rb–Sr, Sm–Nd and Pb–Pb), isotope geochemistry and evolution of the granites and andesite hosting Mohar cauldron, Bundelkhand Granite Complex, Shivpuri District, Central India. Exploration and Research for Atomic Minerals 21, 103–116.
Pati, J.K., Patel, S.C., Pruseth, K.L., Malviya, V.P., Arima, M., Raju, S., Pati, P., Prakash, K., 2007. Geology and geochemistry of giant quartz veins from the Bundelkhand Craton, central India and their implications. Journal of Earth System Sciences 116, 497–510.
Pearce, J.A., 1983. Role of sub-continental lithosphere in magma genesis at active continental margins. In: Hawkesworth, C.J., Norry, M.J. (Eds.), Continental basalts and Mantle Xenoliths. Shiva Press, Nantvach, U.K, pp. 230–249.
Pearce, J.A., 2003. Supra-subduction zone ophiolites: the search for modern analogues. In: Dilek, Y., Newcomb, S. (Eds.), Geological Society of America Special Paper, Ophiolite Concept and the Evolution of Geological Thought, vol. 373, pp. 269–293.
Pearce, J.A., 2008. Geochemical fingerprinting of oceanic basalts with applications to ophiolite classification and the search for Archean oceanic crust. Lithos 100, 14–48.
Pearce, J.A., Peate, D.W., 1995. Tectonic implications of the composition of volcanic arc magmas. Annual Reviews of Earth and Planetary Sciences 23, 251–285.
Pearce, J.A., Parkinson, I.J., 1993. Trace element models for mantle melting: application to volcanic arc petrogenesis. Special Publication of Geological Society of London 76, 373–403.
Pearce, J.A., Barker, P.F., Edwards, S.J., Parkinson, I.J., Leat, P.T., 2000. Geochemistry and tectonic significance of peridotites from the South Sandwich arc-basin system, South Atlantic. Contributions to Mineralogy and Petrology 139, 36–53.
Pearce, J.A., 2014. Geochemical fingerprinting of the earth's oldest rocks. Geology 42, 175–176.
Pearce, J.A., Norry, M.J., 1979. Petrogenetic implications of Ti, Zr, Y, and Nb. Variations in volcanic rocks. Contributions to Mineralogy and Petrology 69, 33–47.
Perfit, R., Gust, D.A., Bence, A.E., Arculus, R.J., Taylor, S., 1980. Chemical characteristics of island-arc basalts: implications for mantle sources. Chemical Geology 30, 227–256.
Pirajno, F., 2000. Ore Deposits and Mantle Plumes. Kluwer Academic Publishers, London, p. 556.
Polat, A., 2013. Geochemical variations in Archean volcanic rocks, southwestern Greenland: traces of diverse tectonic settings in the early Earth. Geology 41, 379–380.
Polat, A., Kerrich, R., 2006. Reading the geochemical fingerprints of Archean hot subduction volcanic rocks: evidence for accretion and crustal recycling in a mobile tectonic regime. American Geophysical Union Geophysical Monograph Series 164, 189–213.
Polat, A., Hofmann, A.W., Rosing, M., 2002. Boninite-like volcanic rocks in the 3.7–3.8 Ga Isua greenstone belt, West Greenland: geochemical evidence for intra-oceanic subduction zone processes in the Earth. Chemical Geology 184, 231–254.
Polat, A., Fryer, B., Samson, I.M., Weisener, C., Appel, P.W.U., Frei, R., Windley, B.F., 2011. Geochemistry of ultramafic rocks and hornblendite veins in the Fiskenæsset layered anorthosite complex, SW Greenland: evidence for hydrous upper mantle in the Archean. Precambrian Research 214–215, 124–153.
Prasad, M.H., Hakim, A., Krishna Rao, B., 1999. Metavolcanic and metasedimentary inclusions in the Bundelkhand Granitic Complex in Tikamgarh district, MP. Journal of the Geological Society of India 54, 359–368.
Rajamani, V., Shivkumar, K., Hanson, G.N., Shirey, S.B., 1985. Geochemistry and petrogenesis of amphibolites from the Kolar schist belt, South India: evidence for ultramafic magma generation by low percent melting. Journal of Petrology 26, 92–123.
Rajanikanta Singh, M., Manikyamba, C., Sohini, Ganguly, Jyotisankar, Ray, Santosh, M., Dhanakumar Singh, Th, Chandan Kumar, B., 2017. Paleoproterozoic arc basalt-boninite-high magnesian andesite-Nb enriched basalt association from the Malangtoli volcanic suite, Singhbhum Craton, eastern India: geochemical record for subduction initiation to arc maturation continuum. Journal of Asian Earth Sciences 134, 191–206.
Rao, M.J., Poornachandra Rao, G.V.S., Widdowson, M., Kelley, S.P., 2005. Evolution of Proterozoic mafic dyke swarms of the Bundelkhand Granite Massif, Central India. Current Science 88, 502–506.
Ray, J.S., 2006. Age of the Vindhyan Supergroup: a review of recent findings. Journal of Earth System Sciences 115, 149–160.
Ray, L., Nagaraju, P., Singh, S.P., Ravi, G., Roy, S., 2015. Radioelemental, petrological and geochemical characterization of the Bundelkhand Craton, central India: implication in the Archean geodynamic evolution. International Journal of Earth Sciences (Geologische Rundschau) 105, 1085–1107.
Rollinson, H., 1999. Petrology and geochemistry of metamorphosed komatiites and basalts from the Sula Mountains greenstone belt, Sierra Leone. Contributions to Mineralogy and Petrology 134, 86–101.
Ross, P.-S., Bedard, J.H., 2009. Magmatic affinity of modern and ancient sub-alkaline volcanic rocks determined from trace element discriminant diagrams. Canadian Journal of Earth Sciences 46, 823–839.
Richards, J.P., Ullrich, T., Kerrich, R., 2006. The late-Miocene-Quaternary Antofalla volcanic complex, southern Puna, NW Argentina: protracted history, diverse petrology, and economic potential. Journal of Volcanology and Geothermal Research 152, 197–239.
Rudnick, R.L., 1995. Making of continental crust. Nature 378, 571–578.
Rudnick, R.L., Gao, S., 2003. Composition of the continental crust. Treatise on Geochemistry 3, 1–64.
Said, N., Kerrich, R., Cassidy, K., Champion, D.C., 2012. Characteristics and geodynamic setting of the 2.7 Ga Yilgarn heterogeneous plume and its interaction with continental lithosphere: evidence from komatiitic-basalt and basalt geochemistry of the Eastern Goldfields Super terrane. Australian Journal of Earth Sciences 59, 1–27.
Saha, L., Frei, D., Gerdes, A., Pati, J.K., Sarkar, S., Patole, V., Bhandari, A., Nasipuri, P., 2016. Crustal geodynamics from the Archean Bundelkhand Craton, India: constraints from zircon U–Pb–Hf isotope studies. Geological Magazine 153, 179–192.
Saha, L., Pant, N.C., Pati, J.K., Upadhyay, D., Berndt, J., Bhattacharya, A., Satyanarayanan, M., 2011. Neoarchean high-pressure margarite-phengitic muscovite-chlorite corona mantled corundum in quartz-free high-Mg, Al phlogopite–chlorite schists from the Bundelkhand Craton, north central India. Contributions to Mineralogy and Petrology 161, 511–530.
Santosh, M., Qiong-Yan, Yang, Shaji, E., Tsunogae, T., Ram Mohan, M., Satyanarayanan, M., 2015. An exotic Mesoarchean microcontinent: the Coorg Block, southern India. Gondwana Research 27, 165–195.
Santosh, M., Teng, X.M., He, X.F., Tang, L., Yang, Q.Y., 2016. Discovery of Neoarchean suprasubduction zone ophiolite suite from Yishui Complex in the north China Craton. Gondwana Research 38, 1–27.
Santosh, M., Hu, C.N., He, X.F., Li, S.S., Tsunogae, T., Shaji, E., Indu, G., 2017. Neoproterozoic arc magmatism in the southern Madurai block, India: subduction, relamination, continental outbuilding, and the growth of Gondwana. Gondwana Research 45, 1–42.
Sarkar, A., Paul, D.K., Potts, P.J., 1996. Geochronology and geochemistry of the mid-Archean trondhjemitic gneisses from the Bundelkhand Craton, Central India. Recent Researches in Geology 16, 76–92.
Saunders, A.D., Norry, M.J., Tarney, J., 1991. Fluid influence on the trace element compositions of subduction zone magmas. Royal Society of London Philosophical Transactions, Ser. A 335, 377–392.

Schandl, E.S., Gortol, M.P., 2002. Application of high field strength elements to discriminate tectonic settings in VMS environments. Economic Geology 97, 377–397.
Sharma, K.K., 2000. Evolution of Archean Palaeoproterozoic crust of the Bundelkhand Craton, northern Indian shield. Research highlights in earth system science. In: Verma, O.P., Mahadevan, T.M. (Eds.), DST Special Publication 1, Indian Geological Congress, pp. 95–105.
Sharma, R., 2009. Cratons and Fold Belts in India. Lecture Notes in Earth Sciences, vol. 127. Springer, p. 304.
Shchipansky, A.A., Khodorevskaya, L.I., Slabunov, A.I., 2012. The geochemistry of and isotopic age of eclogites from the Belomorian Belt (Kola Peninsula): evidence for subducted Archean oceanic crust. Russian Geology and Geophysics 53, 262–280.
Singh, S.P., 2012. Archean geology of Bundelkhand Craton, central India: an overview. Gondwana Geological Magazine Special Volume 13, 125–140.
Singh, S.P., Dwivedi, S.B., 2009. Garnet sillimanite –cordierite –quartz bearing assemblages from the early Archean supracrustal rocks of Bundelkhand Massif Central India. Current Science 97, 103–107.
Singh, S.P., Bhattacharya, A.R., 2010. Signatures of Archean E-W crustal-scale shears in the Bundelkhand Massif, Central India: an example of vertical ductile shearing. E-Journal, Earth Science India 3, 217–225.
Singh, S.P., Dwivedi, S.B., 2015. High grade metamorphism in the Bundelkhand Massif and its implications on Mesoarchean crustal evolution in Central India. Journal of Earth System Science 124, 197–211.
Singh, S.P., Bhattacharya, A.R., 2017. N-S crustal shear system in the Bundelkhand massif: a unique crustal evolution signature in the northern Indian Peninsula. Journal Earth System Sciences (in press, vide manuscript No. JESS-D-16–00633R3). http://www.ias.ac.in/listing/forthcoming/jess.
Singh, S.P., Singh, M.M., Srivastava, G.S., Basu, A.K., 2007. Crustal evolution in Bundelkhand area, Central India. Journal of Himalayan Geology 28, 79–101.
Singh, V.K., Slabunov, A., 2015. The Central Bundelkhand Archean greenstone complex, Bundelkhand Craton, central India: geology, composition, and geochronology of supracrustal rocks. International Geology Review 57, 1349–1364.
Singh, V.K., Slabunov, A., 2016. Two types of Archean supracrustal Belts in the Bundelkhand Craton, India: geology, geochemistry, age and implication for Craton crustal evolution. Journal of the Geological Society of India 88, 533–672.
Slabunov, A., Nazarova, D., Li, X., Singh, V.K., 2013. The role of the Paleoarchean continental crust in the Bundelkhand Craton, Central India: the results of Sm-Nd and U-Pb isotopic studies. In: Singh, V.K., Chandra, R. (Eds.), International Association for Gondwana Research Conference Series No. 16, 3rd International Conference Precambrian Continental Growth and Tectonism, Jhansi, India, pp. 178–179.
Smithies, R.H., Van Kranendonk, M.J., Champion, D.C., 2005. It started with a plume–early Archean basaltic protocontinental crust. Earth and Planetary Science Letters 238, 284–297.
Song, X.-Y., Qi, H.-W., Robinson, P.T., Zhou, M.-F., Cao, Z.-M., Chen, L.-M., 2008. Melting of the subcontinental lithospheric mantle by the Emeishan mantle plume; evidence from the basal alkaline basalts in Dongchuan, Yunan, Southwestern China. Lithos 100, 93–111.
Sproule, R.A., Lesher, C.M., Ayer, J.A., Thurston, P.C., Herzberg, C.T., 2002. Spatial and temporal variation in the geochemistry of komatiites and komatiitic basalts in the Abitibi greenstone belt. Precambrian Research 115, 153–186.
Stern, R.J., Johnson, P., 2010. Continental lithosphere of the Arabian Plate: a geologic, petrologic, and geophysical synthesis. Earth-science Reviews 101, 29–67.
Subramanyam, K.S.V., Balaram, V., Roy, P., Satyanarayanan, M., Sawant, S.S., 2013. Problems involved in using improper calibration CRMs in geochemical analyses – a case study on mafic rocks of Boggulakonda Pluton, East of Cuddapah Basin, India. MAPAN-Journal of Meteorological Society of India 28, 1–9.
Sun, S.S., Nesbitt, R.W., 1978. Petrogenesis of Archean ultrabasic and basic volcanics: evidence from rare earth elements. Contributions to Mineralogy and Petrology 65, 301–325.
Sun, S.S., McDonough, W.F., 1989. Chemical and isotopic systematics of oceanic basalts: implications for mantle composition and processes. Magmatism in the Ocean Basin. Geological Society Special Publication 42, 313–345.
Tatsumi, Y., Hamilton, D.L., Nesbitt, R.W., 1986. Chemical characteristics of fluid phase from the subducted lithosphere: evidence from high-pressure experiments and natural rocks. Journal of Volcanology and Geothermal Research 29, 293–309.
Tatsumi, Y., 2005. The subduction factory: how it operates in the evolving earth. Geological Society of America Today 15, 4–10.
Taylor, S.R., McLennan, S.M., 1985. The Continental Crust: its Composition and Evolution. Blackwell Scientific Publication, Carlton, 312 pp.
Wang, Q., Wyman, D.A., Xu, J., Dong, Y., Vasconcelos, P.M., Pearson, N., Wan, Y., Dong, H., Li, C., Yu, Y., Zhu, T., Feng, X., Zhang, Q., Zi, F., Chu, Z., 2008. Eocene melting of subducting continental crust and early uplifting of central Tibet: evidence from central-western Qiangtang high-K calc-alkaline andesites, dacites and rhyolites. Earth and Planetary Science Letters 272, 158–171.
Weaver, B.L., Tarney, J., 1981. Lewisian Gneiss geochemistry and Archean crustal development models. Earth and Planetary Science Letters 55, 171–180.
Winchester, J.A., Floyd, P.A., 1977. Geochemical discrimination of different magma series and their differentiation products using immobile elements. Chemical Geology 20, 325–343.
Woodhead, J., Eggins, S., Gamble, J., 1993. High field strength and transition element systematics in island arc and back arc basin basalts: evidence for multi-phase melt extraction and a depleted mantle wedge. Earth and Planetary Science Letters 114, 491–504.
Xie, Q., Kerrich, R., Fan, J., 1993. HFSE/REE fractionations recorded in the three komatiite–basalt sequence, Archean Abitibi belt: implications for multiple plume sources and depth. Geochimica et Cosmochimica Acta 57, 4111–4118.
Xiao, W.J., Santosh, M., 2014. The western Central Asian Orogenic Belt: a window to accretionary orogenesis and continental growth. Gondwana Research 25, 1429–1444.
Yang, Q.Y., Santosh, M., Collins, A.S., Teng, X.M., 2016. Microblock amalgamation in the North China Craton: evidence from Neoarchean magmatic suite in the western margin of the Jiaoliao Block. Gondwana Research 31, 96–123.
Yang, Q.Y., Santosh, M., 2017. The building of an Archean microcontinent: evidence from the North China Craton. Gondwana Research. https://doi.org/10.1016/j.gr.2017.01.003.
Zhai, M.G., Santosh, M., 2011. The early Precambrian odyssey of the North China Craton: a synoptic overview. Gondwana Research 20, 6–25.